Drug Design, Development and Therapy

Dovepress
Taylor & Francis Group

Open Access Full Text Article

ORIGINAL RESEARCH

Mechanisms of Magnoliae Officinalis Cortex Volatile Oil in Alleviating 5-Fluorouracil-Induced Mucositis via Multi-Omics Approaches

Jing-Nan Zhang[1,*], Ke-Di Li[1,*], Zhang-Jing Cao[1], Li-Yue Xu[1], Xiao-Lan Zhao[1], Fei Tang[1], Fu Peng[2], Cheng Peng[1], Hui Ao[1]

[1]State Key Laboratory of Southwestern Chinese Medicine Resources, School of Pharmacy, Chengdu University of Traditional Chinese Medicine, Chengdu, 611137, People's Republic of China; [2]Department of Pharmacology, Key Laboratory of Drug-Targeting and Drug Delivery System of the Education Ministry, Sichuan Engineering Laboratory for Plant-Sourced Drug and Sichuan Research Center for Drug Precision Industrial Technology, West China School of Pharmacy, Sichuan University, Chengdu, 610041, People's Republic of China

*These authors contributed equally to this work

Correspondence: Hui Ao; Cheng Peng, State Key Laboratory of Southwestern Chinese Medicine Resources, School of Pharmacy, Chengdu University of Traditional Chinese Medicine, Chengdu, 611137, People's Republic of China, Email aohui2005@126.com; pengchengcxy@126.com

Purpose: Chemotherapy-induced mucositis (CIM) causes severe gastrointestinal symptoms in cancer patients. Magnoliae Officinalis Cortex, a traditional medicine, has demonstrated therapeutic promise in mitigating intestinal mucositis and gastrointestinal disorders, with advantages including marked efficacy and low adverse effect profiles compared to conventional pharmacotherapies. However, the therapeutic potential and mechanisms of the volatile oil of Magnoliae Officinalis Cortex (MagO) against CIM remain elusive. This study aimed to investigate the protective effects and mechanisms of MagO against 5-Fluorouracil (5-FU)-induced mucositis in mice via integrated multi-omics approaches.

Methods: CIM model was established in ICR mice via intraperitoneal injection of 5-FU. The therapeutic effect of MagO on 5-FU-induced CIM was evaluated by monitoring body weight, diarrhea score, spleen index, ileum histopathology, and measuring DAO, D-LA, and inflammatory cytokines levels in serum. Metabolites and gut microbiota were analyzed through non-targeted metabolomics and 16S rDNA sequencing. Furthermore, potential mechanisms of MagO were assessed via GC-MS, network pharmacology, molecular docking, Western blot, and RT-qPCR.

Results: MagO ameliorated 5-FU-induced intestinal mucosal injury and barrier dysfunction, as evidenced by significantly increased body weight rate reduced diarrhea scores, and alleviated ileum tissue damage. It also decreased IL-1β, IL-6, TNF-α, D-LA, and DAO levels in serum. Furthermore, MagO restored gut microbiota composition and metabolite profiles, specifically modulated the arachidonic acid metabolism by promoting PGE2 synthesis and upregulating EP2 and EP4 expressions. Mechanistic studies demonstrated that MagO exerted anti-CIM effects through inhibition of the PI3K/AKT signaling pathway, upregulation of Bcl-2 and intestinal barrier proteins (ZO-1, Occludin) expressions, and downregulation of Bax expression.

Conclusion: MagO mitigated CIM by modulating the PI3K/AKT signaling pathway and the PGE2/EP2/EP4 axis, restoring gut microbiota and metabolites composition, reducing apoptosis, and improving intestinal permeability.

Keywords: Magnoliae Officinalis Cortex volatile oil, 5-fluorouracil, CIM, PI3K/AKT signaling pathway, prostaglandin E2

Introduction

Chemotherapy-induced mucositis (CIM), a common condition characterized by the breakdown of mucosal barriers, is a significant adverse reaction observed in cancer patients undergoing chemotherapy.[1] Symptoms of mucositis may include diarrhea, rectal bleeding, pain, vomiting, and anorexia, often necessitating chemotherapy interruption or dose reduction, thus negatively impacting patient survival outcomes.[2] Diarrhea is a predominant manifestation of CIM, affecting the entire gastrointestinal tract, with approximately 10% of advanced cancer patients experiencing its effect.[3,4] 5-Fluorouracil (5-FU)

Received: 3 January 2025
Accepted: 19 July 2025
Published: 29 August 2025

Graphical Abstract

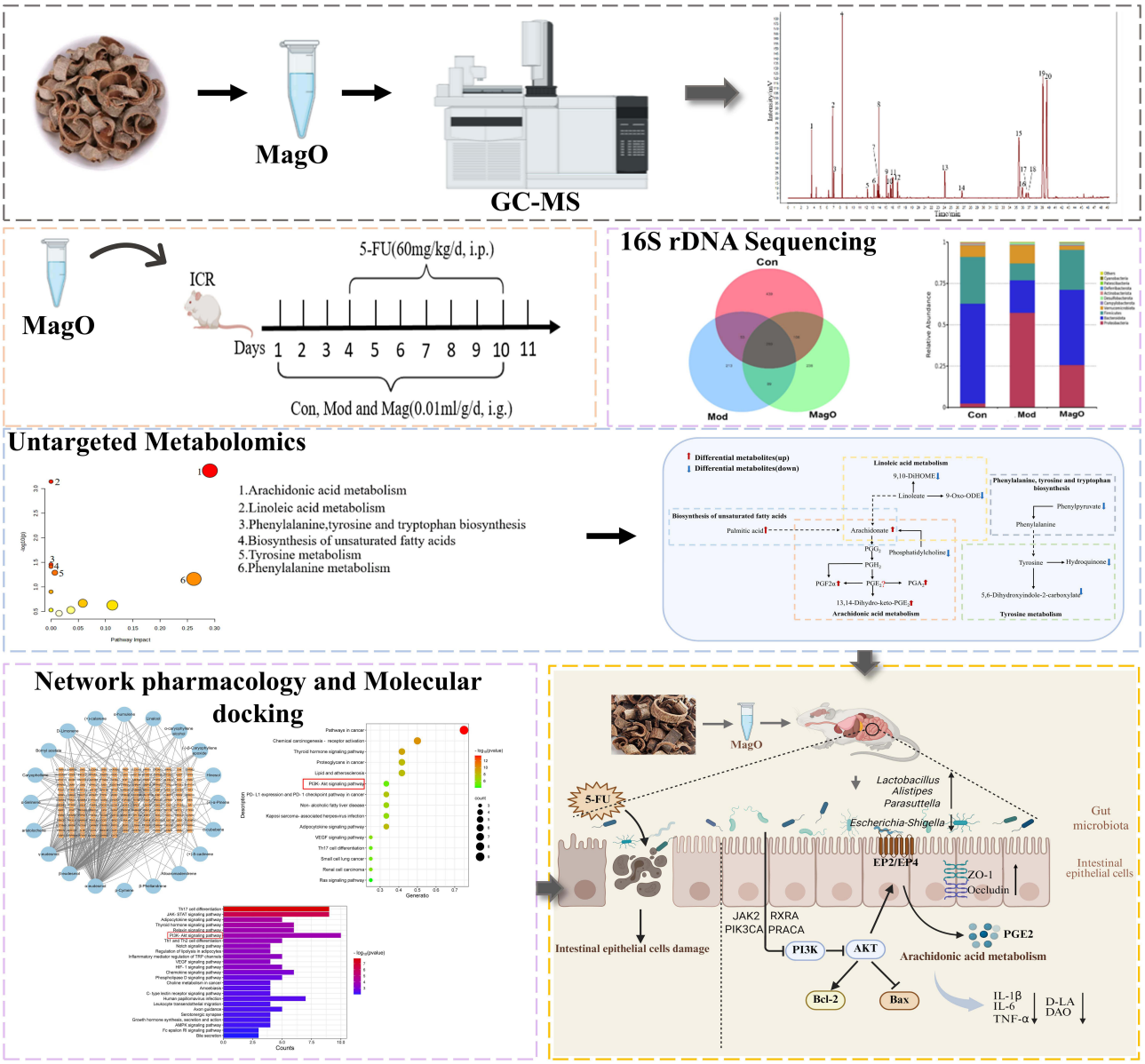

is commonly used for treating colorectal cancer, gastrointestinal tumors, and breast cancer.[5–8] However, 50%~80% of patients on 5-FU develop mucositis, limiting its safety and clinical use.[9] 5-FU targets proliferating cells, notably the rapidly dividing intestinal mucosal cells, causing epithelial vacuolation, crypt cell apoptosis, and excessive mucin secretion.[10] It inhibits thymidylate synthase, disrupts DNA synthesis, and induces apoptosis of intestinal epithelial cells, leading to mucositis.[11] Additionally, 5-FU-induced mucositis is often linked to increased secretion of pro-inflammatory cytokines (TNF-α, IL-1β and IL-6), worsening the condition.[12,13]

Volatile oils from Chinese herbs are increasingly recognized for their pharmacological benefits in relieving CIM and diarrhea.[14–17] Magnoliae Officinalis Cortex is commonly called Houpo, a traditional Chinese herb, has been used in treating gastrointestinal diseases for centuries.[18] Studies have shown that its decoction had a significant effect on 2,4,6-trinitrobenzene sulfonic acid (TNBS)-induced ulcerative colitis. Additionally, it regulated gut microbiota, suppressed inflammation, and

promoted intestinal mucosal repair.[19] The main components of Magnoliae Officinalis Cortex include magnolol, honokiol, and volatile oil.[20] Magnolol has been found to effectively alleviate castor oil-induced acute diarrhea and improve DSS-induced colitis by activating colonic AHR through tryptophan metabolism.[21,22] Furthermore, honokiol regulated gastrointestinal motility by inhibiting the isolated ileum in guinea pigs treated with ACH or $CaCl_2$, providing therapeutic effects for gastrointestinal disorders.[23] Current studies have demonstrated that MagO exhibits multiple biological activities including anti-inflammatory, antibacterial, antioxidant, and gastrointestinal regulatory effects, demonstrating potential in treating CIM.[24] Additionally, Zhang et al[25] demonstrated that MagO protected against dextran sulfate sodium (DSS)-induced ulcerative colitis by restoring intestinal histopathology, improving spleen index and colon mass per unit length in mice, reducing colonic levels of pro-inflammatory cytokines (IL-6, IL-1β, TNF-α), and enhancing intestinal mucosal barrier function through upregulated expressions of tight junction proteins (claudin-1 and occludin). However, the effectiveness of MagO in improving intestinal mucosal barrier and its mechanisms remained inconclusive. Based on these results, we designed experiments to explore MagO' s protective effects against 5-FU-induced mucositis and its mechanisms. We evaluated therapeutic effects by measuring diarrhea scores, body weight changes, spleen index, and ileum histopathology. Gut microbiota changes were analyzed via 16S rDNA sequencing, and fecal metabolites by LC-MS/MS. MagO composition was characterized using GC-MS, and potential targets were predicted through network pharmacology analysis, validated by molecular docking, RT-qPCR and Western Blot assays. This study explores MagO's protective effects against 5-FU-induced mucositis, aiming to provide a theoretical foundation for future research on the treatment of CIM.

Materials and Methods

Reagents and Chemicals

Magnoliae Officinalis Cortex, collected from Dujiangyan, Sichuan (A230602), was authenticated by Associate Professor Lu Chen of the College of Pharmacy at Chengdu University of Traditional Chinese Medicine as the dried bark of *Magnolia officinalis* Rehd. et Wils.(Specimen number: R82-7). 5-FU injection was obtained from Tianjin Jin Yao Pharmaceutical Co., Ltd. (Tianjin, China). Sodium carboxymethyl cellulose was sourced from Macklin Biochemical Co., Ltd. (Shanghai, China). Chromatographic-grade hexane was supplied by Chengdu Kelong Chemical Reagent Factory (Chengdu, China). Loperamide was provided by Xian Janssen Pharmaceutical Ltd. (Xian, China). The D-lactic acid (D-LA) assay kit (Cat. No. ADS-F-T017) and diamine oxidase (DAO) assay kit (Cat. No. ADS-W-YH007-96) were procured from Jiangsu Adison Biological Technology Co., Ltd. (Yancheng, China). Enzyme-linked immunosorbent assay (ELISA) kits for tumor necrosis factor-alpha (TNF-α), interleukin-6 (IL-6), interleukin-1 beta (IL-1β), and prostaglandin E2 (PGE2) were purchased from Jiangsu Meimian Industrial Co., Ltd. (Yancheng, China).

Extraction of MagO

MagO was extracted via steam distillation following the procedures outlined in relevant literature and the 2020 *Chinese Pharmacopoeia* (Volume IV, Method A). Initially, Magnoliae Officinalis Cortex was finely ground into powder. A 300 g portion of this powder was placed into a 3000 mL round-bottom flask, and 2400 mL of distilled water was added. The mixture was soaked for 2 hours to facilitate initial extraction. Subsequently, the flask was connected to a steam distillation apparatus, and continuous extraction was performed for 4 hours until the oil yield stabilized. The extracted MagO was collected and stored at 4 °C in a sealed container. The extraction yield was calculated using the formula:

$R = (V/m) \times 100\%$. R represented the extraction rate, V represented the volume, and m represented the mass.

GC-MS Analysis of MagO

MagO was analyzed using gas chromatography-mass spectrometry (GC-MS) on an Agilent 7890A-5975C instrument (Agilent, USA) equipped with an HP-5MS capillary column (30 m × 250 μm × 0.25 μm). Helium served as the carrier gas at a flow rate of 1.0 $mL \cdot min^{-1}$, and the injection volume was 1 μL. The samples were diluted 1:100 in hexane and introduced with a split ratio of 80:1. Electron ionization was conducted at 70 eV, with the ion source and quadrupole temperatures set at 230 °C and 150 °C, respectively. A solvent delay of 3 minutes was applied. The GC oven temperature

program initiated at 50 °C (held for 3 minutes), ramped up at 8.0 °C·min^{-1} to 140 °C (held for 5 minutes), then increased at 0.5 °C·min^{-1} to 150 °C, and finally elevated at 5 °C·min^{-1} to 200 °C, resulting in a total run time of 49.25 minutes. Identification of MagO components was achieved by comparing their mass spectra with those in the National Institute of Standards and Technology (NIST) database. The percentage composition of each component was calculated by normalizing its peak area to the total ion current (TIC).

Animals and Treatment

Specific pathogen-free (SPF) grade ICR mice (weighing 20±2 g) were procured from Chengdu Dossy Experimental Animals Co., Ltd. The animals were housed under standard laboratory conditions: temperature maintained at 23 ± 2 °C, humidity at 50% ± 5%, and a 12-hour light/dark cycle, with unrestricted access to standard chow and water. All experimental procedures were approved by the Animal Ethics Committee of Chengdu University of Traditional Chinese Medicine (Approval No.: 2022003021) and adhered strictly to institutional guidelines for the care and use of laboratory animals. After a 3-day acclimation period, 48 male mice were randomly assigned to six groups (n = 8 per group): Control (Con), 5-FU model (Mod), loperamide (Lop), and low-, medium-, and high-dose MagO groups (MagO-L at 25 μL·kg^{-1}, MagO-M at 50 μL·kg^{-1}, and MagO-H at 100 μL·kg^{-1}, respectively). Animals were randomly assigned to different groups. Researchers were blinded to group allocations during data collection and analysis. The MagO emulsions of varying concentrations were prepared by dissolving the compound in a 0.3% sodium carboxymethyl cellulose solution for administration to the respective treatment groups. Both the Con and Mod groups received an equivalent volume of the 0.3% sodium carboxymethyl cellulose solution once daily for 10 consecutive days. From day 4 to day 10, the Mod, Lop, and MagO groups were administered intraperitoneal injections of 5-FU at a dose of 60 mg·kg^{-1}·day^{-1}, while the Con group received the same volume of normal saline. On the final day of the experiment, fecal matter, serum, and ileum tissues were collected and stored at −80 °C for subsequent analyses.

Monitoring of Body Weights, Diarrhea Scores and Spleen Indexes

Throughout the experiment, the body weight of the mice was recorded daily at a consistent time and place, and diarrhea scores were systematically documented. Diarrhea severity was evaluated using the criteria established by Akinobu Kurita:[26] Diarrhea severity was assessed using a scoring system ranging from 0 to 3: a score of 0 indicated normal stools with no diarrhea; 1 signified mild diarrhea characterized by moist or soft stools; 2 corresponded to moderate diarrhea with wet, unformed stools and slight perianal staining; and 3 denoted severe diarrhea with watery stools and significant perianal staining. Daily body weight ratios were calculated based on the mice's weights recorded on day 3 of the experiment. On the final day, mice were humanely euthanized via cervical dislocation, and their spleens were extracted.

The spleen index was determined using the formula:

$$\text{Spleen index} = \text{spleen weight/body weight (mg·g}^{-1}\text{)}.$$

Hematoxylin and Eosin (HE) Staining

An approximately 2 cm segment of the mice's distal ileum was excised and fixed in 4% paraformaldehyde. Following fixation, the tissues were embedded, and 4 μm-thick sections were prepared and stained with hematoxylin and eosin (HE). The pathological alterations in the intestinal tissues were then examined and evaluated using a microscope equipped with a digital camera system (Olympus Optical Co., Ltd., Tokyo, Japan).

Intestinal Permeability

Using commercial assay kits and meticulously following the manufacturer's instructions and protocols, we measured the levels of D-LA and DAO in mice serum.

Enzyme-Linked Immunosorbent Assay (ELISA) Analysis

The concentrations of TNF-α, IL-6, and IL-1β in mice serum, as well as the levels of PGE2 in ileum tissue, were determined using ELISA kits in accordance with the manufacturer's guidelines. All the assays were performed meticulously following the provided protocols to ensure the reliability and reproducibility of the results.

16S rDNA Sequencing Analysis

Total DNA was extracted from mouse fecal samples using the Magnetic Soil and Stool DNA Kit (TianGen, China), and its quality was assessed via 1% agarose gel electrophoresis before diluting to 1 ng/μL. The V3-V4 region of bacterial 16S rDNA was amplified using Phusion High-Fidelity PCR Master Mix (New England Biolabs, USA). Subsequently, the PCR products were extracted from 2% agarose gels, and the PCR products that passed the test were mixed and purified. These purified products were subjected to library construction and sequenced on Illumina NovaSeq platform. The raw sequencing data were then processed through assembling, filtering, and denoising procedures to obtain amplicon sequence variants (ASVs). Finally, species annotation of the ASVs was performed using the QIIME2 software.

Untargeted Metabolomics Analysis

Fecal samples (100 mg) were ground in liquid nitrogen, mixed with 500 μL of 80% methanol-water solution, vortexed, chilled on ice for 5 minutes, and centrifuged at 15,000 g for 20 minutes at 4 °C. The supernatant was diluted with LC-MS-grade water to achieve 53% methanol, centrifuged again, and collected for LC-MS analysis. Metabolites were analyzed using LC-MS/MS, with chromatographic separation carried out on a Vanquish UHPL (Thermo Fisher, Germany) and a Hypesil Gold column (100 mm × 2.1 mm, 1.9 μm) (Thermo Fisher, USA). Analyses were performed using a Q Exactive™HF-X (Thermo Fisher, Germany) mass spectrometer. Compounds with a coefficient of variation (CV) over 30% in Quality control (QC) samples were excluded, finalizing metabolite identification and quantification. Metabolite annotation employed the KEGG (https://www.genome.jp/kegg/pathway.html), HMDB (https://hmdb.ca/metabolites), and LIPIDMaps (http://www.lipidmaps.org/) databases. Multivariate analyses, including principal component analysis (PCA) and partial least squares discriminant analysis (PLS-DA), were performed using metaX software to calculate variable importance in projection (VIP) values. Univariate *t*-tests assessed statistical significance (*P*-values) and fold changes (FC) of metabolites between groups. Metabolites were considered differentially expressed if they met the criteria: VIP > 1, $P < 0.05$, and FC >1.2 or < 0.833.

Network Pharmacology

Based on GC-MS analysis, MagO was found to contain 20 active components. The SMILES representations of these compounds were obtained from the PubChem database (https://pubchem.ncbi.nlm.nih.gov/). Potential targets were predicted using these SMILES formats via the SwissTargetPrediction database (http://www.swisstargetprediction.ch/) and converted into gene names using the UniProt database (https://www.uniprot.org/), removing any duplicates. Additionally, the GeneCards (https://www.genecards.org/) and Online Mendelian Inheritance in Man (OMIM) (https://omim.org/) databases were used to obtain the CIM-related targets with the keywords "enteritis", "colitis", "inflammatory bowel disease", and "diarrhea". Targets common to both MagO and CIM were identified as potential therapeutic targets against 5-FU-induced mucositis. A "component-target" interaction network was constructed using Cytoscape 3.9.0. The interactions among predicted targets were analyzed using the STRING database (https://cn.string-db.org/), selecting Homo sapiens as the species for protein-protein interaction (PPI) analysis. The resulting TSV file was imported into Cytoscape 3.9.0 to create a PPI network. Key targets were identified using the CentiScaPe 2.2 plugin in Cytoscape, based on parameters like degree, betweenness, and closeness. Additionally, Gene Ontology (GO) and Kyoto Encyclopedia of Genes and Genomes (KEGG) enrichment analyses were performed on MagO's potential targets using the "Functional Annotation" tool on the Metascape platform (https://metascape.org/gp/index.html#/main/step1), with significance set at $P < 0.05$. The results were visualized using bubble charts and bar graphs generated on the MicrobiomeAnalyst platform. In the combined analysis of network pharmacology and metabolomics, the "Joint-Pathway Analysis" function of the MetaboAnalyst 6.0 database was utilized. Shared genes and differential metabolites were simultaneously input into the database to identify the pathways they jointly influence. Pathways named after other diseases were excluded, and the top 25 ranked pathways were presented.

Molecular Docking

JAK2, PIK3CA, PRKCA, and RXRA were chosen as the primary molecular docking targets. Available Homo sapiens templates for these targets, including 6VN8, 2RD0, 2GZV, and 4PP3, were retrieved from the Protein Data Bank (PDB,

https://www.rcsb.org/). Virtual docking was conducted using AutoDock Vina software, selecting ligands with the lowest binding energy and optimal orientation. The docking results were then visualized using PyMOL 2.6.0 software.

Reverse Transcription Quantitative Polymerase Chain Reaction (RT-qPCR) Analysis

RNA was reverse-transcribed into cDNA using the M-MLV RT reaction mix with gDNAse (Accurate Biotechnology, China), following the manufacturer's instructions. Quantitative RT-qPCR was performed on an Archimed X4 system (ROCGENE, China) using SYBR Green Pro Taq HS Premix (Accurate Biotechnology, China). Relative mRNA expression levels were determined using the $2^{-\Delta\Delta Ct}$ method. The primer sequences used in this study are listed in Supplementary Table S1.

Western Blot Analysis

To evaluate the expression levels of ZO-1, Occludin, Bax, Bcl-2, P-PI3K/PI3K, and P-AKT/AKT proteins in ileal tissue, Western blot analysis was performed. Ileum tissue samples were initially homogenized in RIPA lysis buffer using a tissue grinder operated at low temperatures (−20 °C) and a frequency of 65 Hz. The homogenization was executed three times, each lasting 120 seconds with a 10-second pause between cycles. Following homogenization, the lysates were centrifuged at 12,000 g for 15 minutes at 4 °C to collect the supernatant. Total protein concentrations were measured using a BCA protein assay kit (Oriscience, China). The samples were added with loading buffer after adjusting the protein concentration and heated in metal bath at 95°C for 5 minutes. The protein samples were then separated on a 10% SDS-PAGE gel and transferred onto PVDF membranes. The membranes were incubated overnight at 4 °C with primary antibodies targeting ZO-1, Occludin (both at 1:1000 dilution; Affinity), Bax, Bcl-2, P-PI3K, PI3K, P-AKT, AKT (all at 1:2000 dilution; Affinity), β-actin (1:6000 dilution; Bioss), and GAPDH (1:6000 dilution; Bioss). Subsequently, the membranes were incubated with a secondary antibody (goat anti-rabbit IgG-HRP; 1:5000 dilution) at 37 °C for 2 hours. Chemiluminescent signals were developed using an ECL kit (Oriscience, China), and the band intensities were analyzed using Image J software.

Immunohistochemistry (IHC) Staining

To evaluate the expression levels of ZO-1, Occludin, EP2, and EP4 (Affinity, China), IHC staining was performed on ileum tissue sections. Images were acquired using a microscope equipped with a digital camera (Olympus Optical Co., Ltd., Tokyo, Japan) and quantitatively analyzed with ImageJ software. To ensure data reliability, three random fields of view from each section were selected, and the mean optical density (MOD) was calculated.

Statistical Analysis

All data are presented as the mean ± standard error of the mean (SEM), and statistical analyses were performed using GraphPad Prism (version 8.0.1). Differences between multiple groups were evaluated using one-way analysis of variance (ANOVA), followed by Dunnett post hoc tests for multiple comparisons. $P < 0.05$ was considered as statistical significance.

Results

Chemical Compositions of MagO

The results of the GC-MS analysis were shown in Figure 1 and Supplementary Table S2. The proportion of each component was obtained by peak area normalization. A total of 20 compounds were identified, accounting for 96.99% area of all the detected chromatographic peaks in MagO, including β-eudesmol (39.085min, 26.75%), α-eudesmol (39.655min, 23.20%), γ-eudesmol (35.378min, 9.82%), p-Cymene (8.312min, 7.13%), (-)-β-Caryophyllene epoxide (24.041min, 4.73%),(+)-calarene (35.899, 4.43%), α-selinene (16.012min, 1.74%), and aristolochene (36.655min, 0.59%).

MagO Improved the Changes of Body Weight Rate, Diarrhea Scores and Spleen Index in 5-FU Induced Mucositis Mice

The experimental workflow was implemented in accordance with the procedures described in the materials and methods section and depicted in Figure 2A. As depicted in Figure 2B and C, starting from day 5 of the experiment (the second day

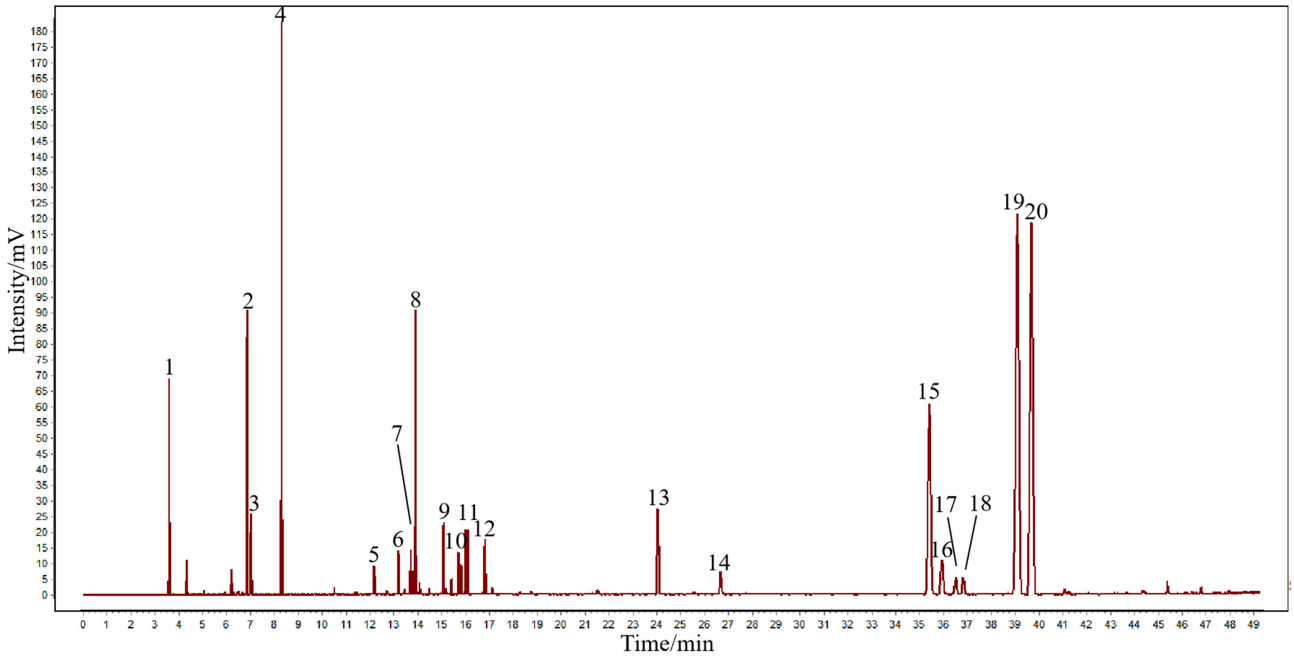

Figure 1 The total ion flow diagram of MagO analyzed by GC-MS. The y-axis represents signal intensity (in parts per thousand of the actual signal), and the x-axis denotes time.

following 5-FU administration), a consistent decline in body weight was observed in the mice. On day 10, the body weight of 5-FU group was significantly reduced compared to the Con group ($P < 0.001$). In contrast, both Lop and MagO-H groups exhibited significantly lower body weight reductions compared to 5-FU group ($P < 0.05$), while no significant differences were observed in MagO-L and MagO-M groups. Moreover, the diarrhea scores in 5-FU group showed a sustained increase relative to the Con group ($P < 0.01$). Notably, Lop and MagO-H groups demonstrated a significant reduction in diarrhea scores compared to the Mod group ($P < 0.05$), with no significant changes observed in MagO-L and MagO-M groups. Additionally, the spleen index was significantly elevated in 5-FU group relative to the Con group ($P < 0.001$). Both of Lop and MagO-H groups were effective in markedly reducing the spleen index compared to 5-FU group ($P < 0.001$, $P < 0.01$), while the MagO-L and MagO-M groups showed no significant differences (Figure 2D). These findings suggested that MagO-H effectively mitigated 5-FU-induced body weight loss, increased diarrhea scores, and elevated spleen index, thereby demonstrating its potential therapeutic efficacy.

MagO Inhibited the Pathological Changes of Ileums in 5-FU Induced Mucositis Mice

As shown in Figure 2E, the intestinal mucosa, villi, and crypt structures in the Con group remained intact, with no observed damage or inflammatory infiltration. In contrast, significant pathological changes were observed in the ileum of 5-FU-induced mice, including villi shortening, shedding, crypt damage, and vacuolization and infiltration of inflammatory cells. Compared to the Mod group, Lop, MagO-M and MagO-H groups showed significant efficacy in alleviating the intestinal damage, with Mag-H group being the most effective. In contrast, MagO-L group did not prominently inhibit the pathological changes in the ileum.

MagO Inhibited the Intestinal Permeability and Levels of Inflammatory Cytokines of Serum in 5-FU Induced Mucositis Mice

As shown in Figure 2F and G, compared to the Con group, 5-FU significantly increased the DAO and D-LA levels in serum ($P < 0.001$), indicating a marked increase in intestinal permeability in mice. Compared to the Mod group, Lop group, as well as MagO-M and MagO-H groups, significantly restored levels of DAO and L-DA. Figure 2H and J demonstrated that 5-FU evidently elevated serum levels of IL-1β, IL-6, and TNF-α ($P < 0.001$) compared to the Con group, indicating an enhanced

https://doi.org/10.2147/DDDT.S515605

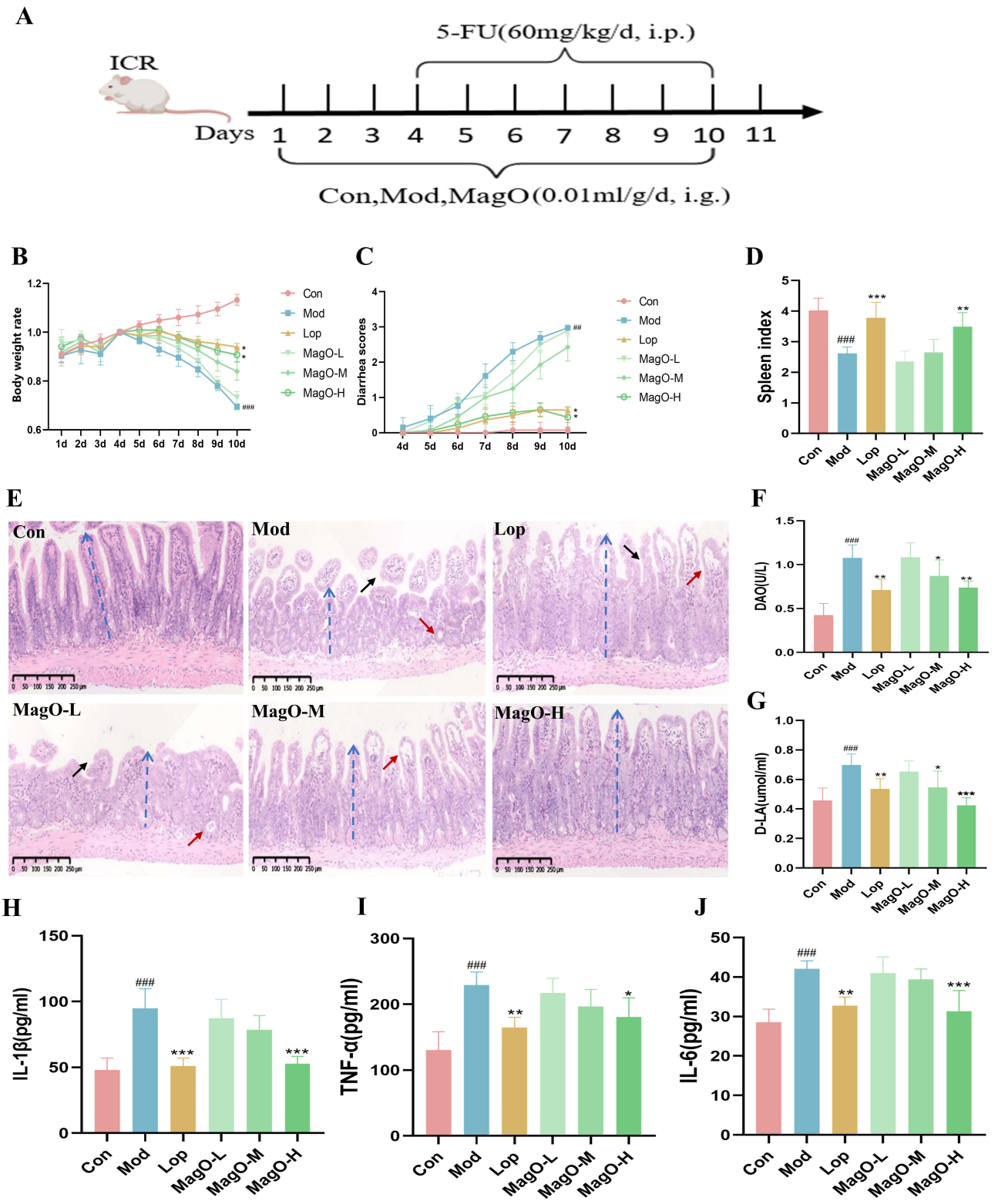

Figure 2 MagO improved 5-FU induced mucositis mice (n=8). (**A**) Experimental framework and treatments. (**B**) Body weight rate. (**C**) Diarrhea scores. (**D**) Spleen index. (**E**) Histological microstructure of ileums (10×magnification) by H&E staining. In (**E**), the blue arrow indicated the villus length and crypt depth, the red arrow indicated the cavitation, the black arrow indicated the intestinal villi injury and loss; scale bar,250 μm. (**F**) DAO. (**G**) D-LA. (**H**) IL-1β.(**I**) TNF-α. (**J**) IL-6. The data were expressed in means ± SEM. $^{*}P < 0.05$, $^{**}P < 0.01$, $^{***}P < 0.001$ vs Mod group; $^{\#\#}P < 0.01$, $^{\#\#\#}P < 0.001$ vs Con group.

https://doi.org/10.2147/DDDT.S515605

inflammatory response. Compared to the Mod group, Lop group and MagO-H group were able to significantly suppress the levels of these inflammatory cytokines.

Effects of MagO on the Gut Microbiota Composition in 5-FU Induced Mucositis Mice

Based on the above pharmacological indicators, MagO-H was selected for 16S rDNA sequencing analysis. The impact of MagO on the gut microbiota composition in fecal samples from 5-FU-induced mice was investigated. A Venn diagram was utilized to represent the OTUs of gut microbiota across different groups. As shown in Figure 3A, 1410 OTUs were shared among the three groups, with 439, 213, and 238 unique OTUs in the Con, the Mod, and MagO groups, respectively. β diversity analysis was employed to compare microbial community composition between different samples; closer distances between samples indicate more similar species composition. As depicted in Figure 3B and C, PCoA and NMDS analyses demonstrated significant separation between the Con and the Mod groups, while MagO group showed a trend toward convergence with the Con group. Alpha diversity analysis was conducted to assess species richness and diversity within each group. As shown in Figure 3D–F, 5-FU significantly reduced the Chao1, Shannon, and Simpson indexes ($P < 0.01$, $P < 0.001$, $P < 0.001$), whereas the MagO treatment group evidently reversed these declines ($P < 0.05$, $P < 0.01$, $P < 0.01$). The relative abundance of gut microbiota at the phylum and genus levels is shown in Figure 3G and H. At the phylum level, compared to the Con group, 5-FU increased relative abundances of *Proteobacteria, Verrucomicrobiota*, and *Desulfobacterota* and decreased the relative abundances of *Bacteroidota, Firmicutes, Actinobacteriota*, and *Patescibacteria*. At the genus level, 5-FU increased the relative abundance of *Escherichia-Shigella*, while decreasing the relative abundances of *Lactobacillus, Bacteroides, Alloprevotella* and others. MagO successfully reversed the changes in microbial relative abundance at both the phylum and genus levels.

Furthermore, MetaStat analysis was employed to identify taxa with statistical significance, focusing on those disrupted by 5-FU and restored by MagO treatment (Figure 3I). A total of 11 taxa were identified. 5-FU significantly increased the relative abundance of *Escherichia-Shigella*, while significantly decreasing the relative abundances of *Lactobacillus, Bacteroides, Alloprevotella, Erysipelatoclostridium, Parasutterella, Alistipes, Enterorhabdus, Colidextribacter*, and *Candidatus_Arthromitus*. MagO treatment significantly reversed these changes. LEfSe analysis further identified taxa with significant differences (LDA score >3), revealing dominant species in each group (Figure 3J). In the Con group, dominant taxa included *Bacteroidales, Bacteroidota, Bacteroidia, Muribaculaceae, Bacilli*, and *Lactobacillaceae*; in MagO group, dominant taxa included *Prevotellaceae, Ruminococcus_torques_group, Butyricimonas_synergistica*, and *Blautia*; but in the Mod group, dominant taxa included *Enterobacterales, Escherichia_Shigella, Gammaproteobacteria, Proteobacteria*, and *Acidaminococcaceae*. These results indicated that MagO effectively reversed 5-FU-induced gut dysbiosis.

Effect of MagO on Fecal Metabolites in 5-FU Induced Mucositis Mice

In this section of the study, a non-targeted metabolomics analysis of fecal samples from the Con group, the Mod group, and MagO groups was performed using LC-MS/MS technology. A total of 995 metabolites in positive ion mode and 683 metabolites in negative ion mode were identified. Principal component analysis (PCA) was used to observe the overall metabolic distribution among the groups. As shown in Figure 4A, there were significant metabolic differences between the Mod group and the Con group, and MagO group still exhibited significant separation from the Mod group, trending toward the Con group. This suggested that MagO might exert therapeutic effects on 5-FU-induced mucositis by modulating metabolite composition. Similarly, Partial least squares discriminant analysis (PLS-DA) was further conducted to screen for differential metabolites between the groups. Figure 4B and C show clear separation between the Con and the Mod groups, as well as between the Mod and MagO groups, indicating that the model was not overfitted and that the established method demonstrated good stability and reproducibility. Differential metabolites were then screened using the criteria of VIP > 1.0, FC > 1.2, or FC < 0.833, with $P < 0.05$. The volcano plots provide a visual representation of the overall distribution of differential metabolites. As shown in Figure 4D and E, in comparison to the Con group, levels of 146 metabolites were downregulated and levels of 37 metabolites were upregulated in the feces of 5-FU-treated mice with mucositis. In comparison to the Mod group, the MagO treatment group downregulated levels of 35 metabolites and upregulated levels of 195 metabolites. Notably, levels of 68 metabolites were simultaneously affected by both 5-FU and

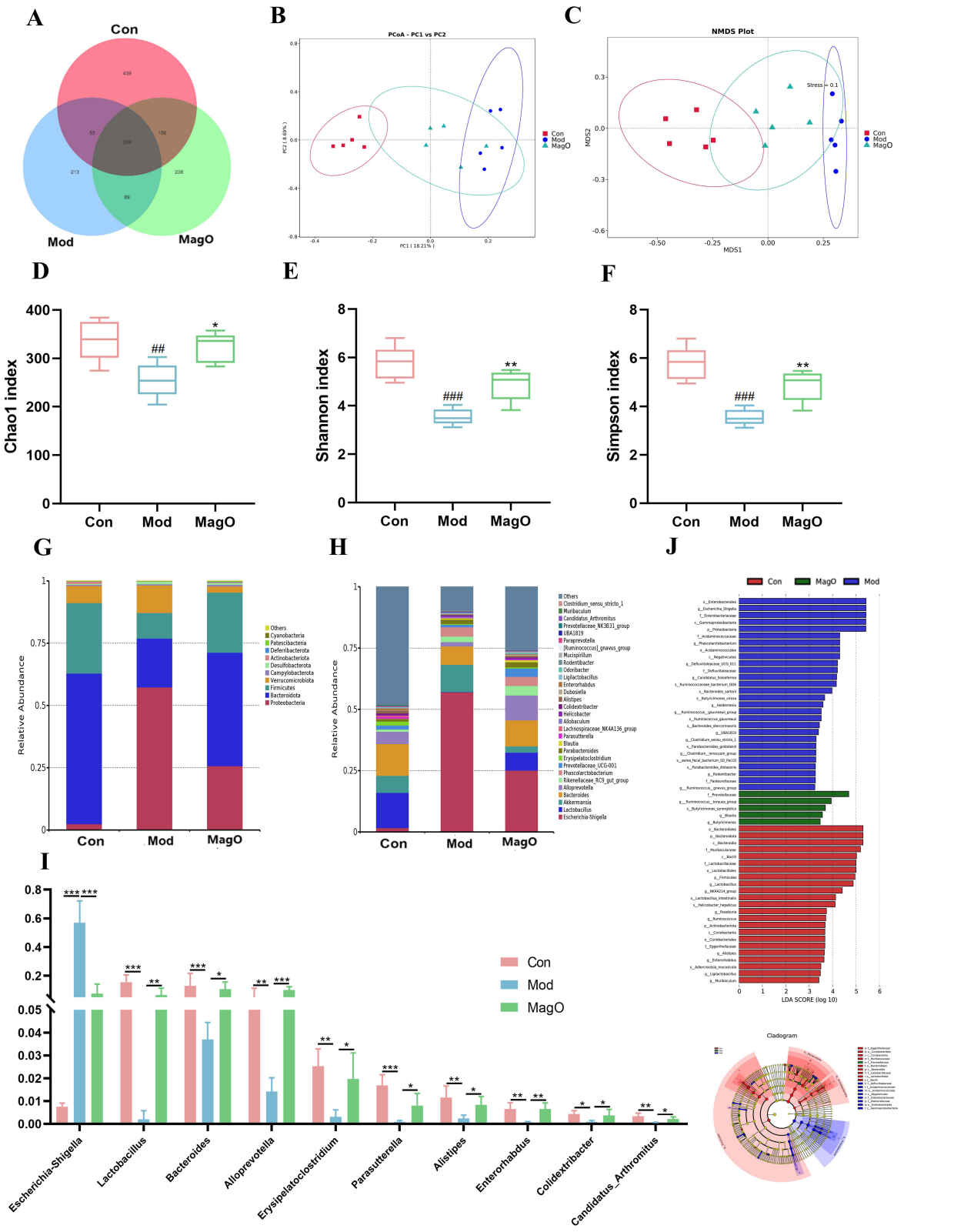

Figure 3 Regulatory role of MagO on the gut microbiota composition in 5-FU induced mucositis mice (n=5). (**A**) Venn diagram showing ASVs in each group. (**B** and **C**) Beta diversity analysis of the gut microbiota utilizing PCoA plot and NMDS plot. (**D**-**F**) Alpha diversity analysis of the gut microbiota utilizing the Chao1, Shannon and Simpson indexes. (**G** and **H**) Map of the relative abundance of species at the phylum, genus levels of each group. (**I**) Species disturbed by 5-FU but restored by MagO at the genus level. (**J**) Taxonomic cladogram generated by linear discriminant analysis (LDA) effect size (LEfSe) of gut microbiota among the three groups. Circle size was proportional to the abundance of the taxon. The data were expressed in means ± SEM.*P < 0.05, **P < 0.01, ***P < 0.001vs. Mod group; $^{\#\#}P$ < 0.01, $^{\#\#\#}P$ < 0.001 vs Con group.

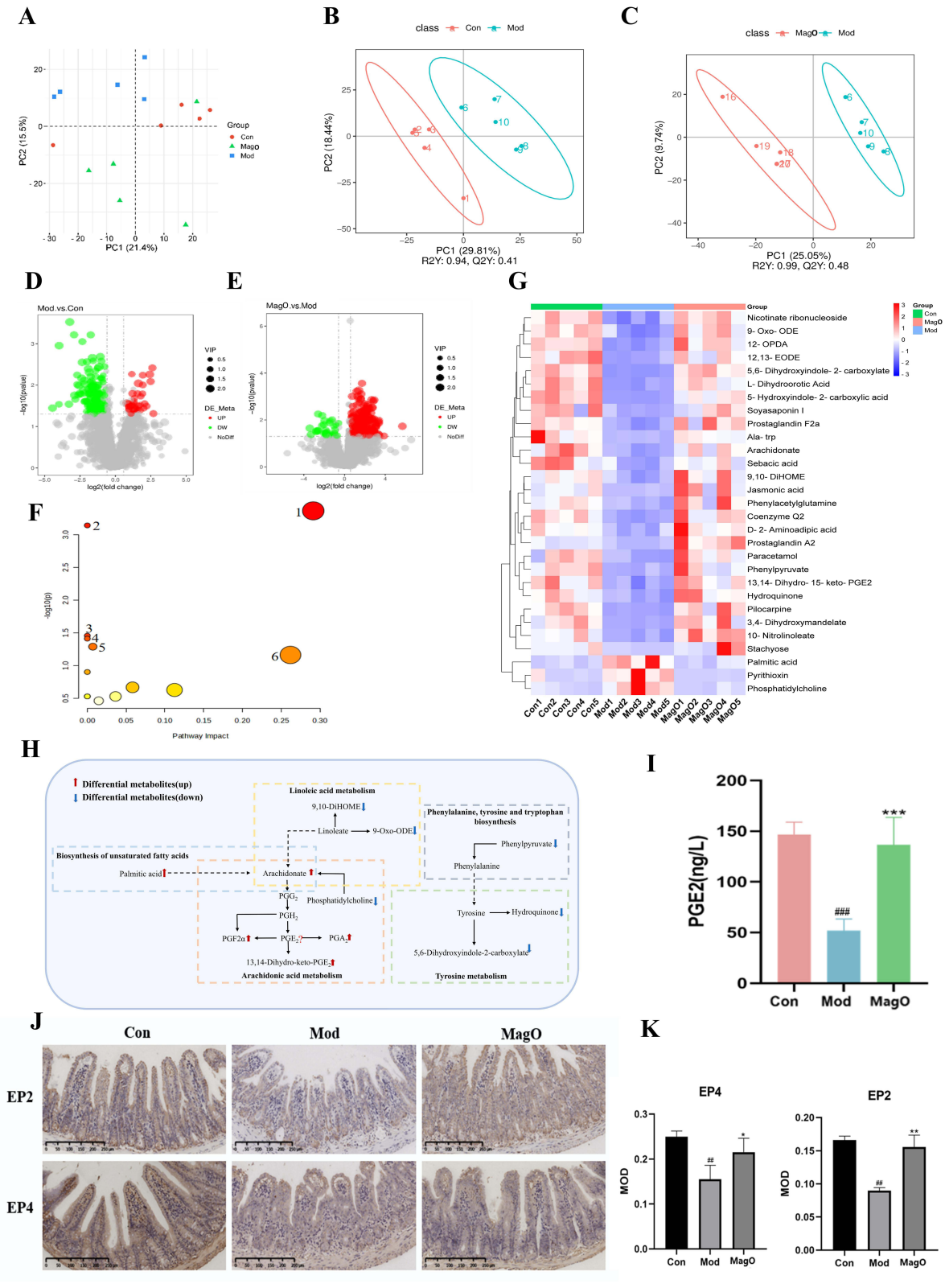

Figure 4 Effect of MagO on fecal metabolites in 5-FU induced mucositis mice (n=5). (**A**) PCA score plot. (**B**) PLS-DA score plot between Con and Mod groups. (**C**) PLS-DA score plot between MagO and the Mod groups. (**D**) The volcano plot of differential metabolites in Mod group vs Con group. (**E**) The volcano plot of differential metabolites in MagO group VS the Mod group. (**F**) Pathway enrichment of differential metabolites altered by MagO.1: Arachidonic acid metabolism.2: Linoleic acid metabolism. 3: phenylalanine, tyrosine and tryptophan biosynthesis.4: Biosynthesis of unsaturated fatty acids.5: Tyrosine metabolism.6: Phenylalanine metabolism. (**G**) The heat map of differential metabolites involved in metabolic pathways. (**H**) The pathways of Arachidonic acid metabolism and PGE2 synthesis metabolism. (**I**) The levels of PGE2 in feces were determined by ELISA kits. (**J** and **K**) Cellular localization and expressions of EP2 and EP4 were assessed using immunohistochemistry (n = 3 per group); scale bar, 250μm. The data were expressed in means ± SEM. $^{*}P < 0.05$, $^{**}P < 0.01$, $^{***}P < 0.001$, vs Mod group; $^{\#\#}P < 0.01$, $^{\#\#\#}P < 0.001$ vs Con.

https://doi.org/10.2147/DDDT.S515605

MagO, with 5-FU downregulating levels of 61 metabolites and upregulating levels of 7 metabolites, all of which were successfully reversed by MagO. To further investigate the mechanisms by which MagO ameliorates 5-FU-induced mucositis, the 68 differential metabolites were subjected to KEGG pathway enrichment analysis. As shown in Figure 4F, MagO significantly regulated several metabolic pathways, including arachidonic acid metabolism, linoleic acid metabolism, phenylalanine, tyrosine, and tryptophan biosynthesis, biosynthesis of unsaturated fatty acids, tyrosine metabolism, and phenylalanine metabolism, with arachidonic acid metabolism identified as the most critical pathway. Additionally, the changes in differential metabolites involved in these metabolic pathways were visualized through a normalized heatmap. As shown in Figure 4G, 5-FU significantly upregulated levels of 3 metabolites (palmitic acid, phosphatidylcholine, pyrithioxin) and downregulated levels of 26 metabolites, including Arachidonate, 13,14-dihydro-15-keto-prostaglandinE2, prostaglandinF2α, and prostaglandin A2.

Construction of Metabolic Pathways and Potential Mechanisms

Based on metabolomics results above, the major metabolic pathway network of MagO-treatment towards 5-FU-induced mucositis was shown in Figure 4H. Arachidonic acid metabolism emerged as the most significant metabolic pathway in MagO's treatment of 5-FU-induced mucositis. 5-FU significantly upregulated three metabolites (palmitic acid, phosphatidylcholine, pyrithioxin) and downregulated 26 metabolites, including Arachidonate, 13,14-dihydro-15-keto-prostaglandinE2, prostaglandinF2α, and prostaglandin A2. Additionally, we investigated whether MagO exerts its effects by modulating the expression of prostaglandinE2 (PGE2) and its receptors EP2 and EP4, we measured PGE2 levels in ileum tissues and assessed the expression of EP2 and EP4 through immunohistochemistry. As shown in Figure 4I, 5-FU significantly downregulated PGE2 level compared to the Con group (P <0.001), whereas MagO significantly restored these levels (P <0.01). Additionally, 5-FU markedly suppressed the expressions of EP2 and EP4 (P <0.01), which was effectively reversed by MagO (P <0.01, P <0.05) (Figure 4J and K).

Correlation Analysis

KEGG pathway analysis identified that MagO significantly modulates pathways including arachidonic acid metabolism, linoleic acid metabolism, and the biosynthesis of phenylalanine, tyrosine, tryptophan, and unsaturated fatty acids. Pearson correlation heat map analysis was used to investigate the relationships between metabolites in these pathways, phenotypic data, and gut microbiota (Figure 5A–C). The analysis revealed significant correlations, particularly highlighting *Escherichia-Shigella*, which were positively associated with inflammatory markers and diarrhea scores, while negatively correlated with spleen index and body weight ratio. In contrast, *Lactobacillus, Alistipes*, and *Parasutterella* exhibited inverse correlations, indicating their protective roles. Additionally, palmitic acid and phosphatidylcholine were positively associated with inflammatory and phenotypic markers, whereas other metabolites like prostaglandin F2a and arachidonic acid were negatively correlated. Finally, we investigated the interactions between the microbiota and metabolites to assess their influence on CIM. *Escherichia-Shigella* showed a notable positive correlation with palmitic acid and phosphatidylcholine and a negative correlation with 7 metabolites including 13,14-Dihydro-15-keto-prostaglandinE2, Arachidonate and ProstaglandinF2α. In contrast, relative abundance of *Lactobacillus* demonstrated an opposite trend in its correlation with levels of metabolites compared to that of *Escherichia-Shigella*. These findings suggested that the therapeutic effects of MagO might be closely associated with arachidonic acid metabolism, with *Escherichia-Shigella, Lactobacillus, Alistipes*, and *Parasutterella* likely playing pivotal roles in this process. Collectively, this indicated that MagO mitigated 5-FU-induced intestinal inflammation, mucosal damage, and diarrhea by regulating microbiota and metabolites.

Network Pharmacology Predicts Potential Mechanisms for MagO Treatment of CIM

To further explore the mechanisms underlying MagO's anti-CIM efficacy, network pharmacology techniques were employed to predict the targets of these key components in MagO and their association with CIM.

A "component-target" network was constructed, revealing that 20 active components of MagO were associated with 175 targets (Figure 6A). Significant active components were identified through node degree screening. Notably, key components of MagO, including β-eudesmol, α-eudesmol, γ-eudesmol, aristolochene, and α-selinene, were highlighted, suggesting their crucial roles in the treatment of mucositis. As illustrated in Figure 6B, 51 overlapping targets were identified between the

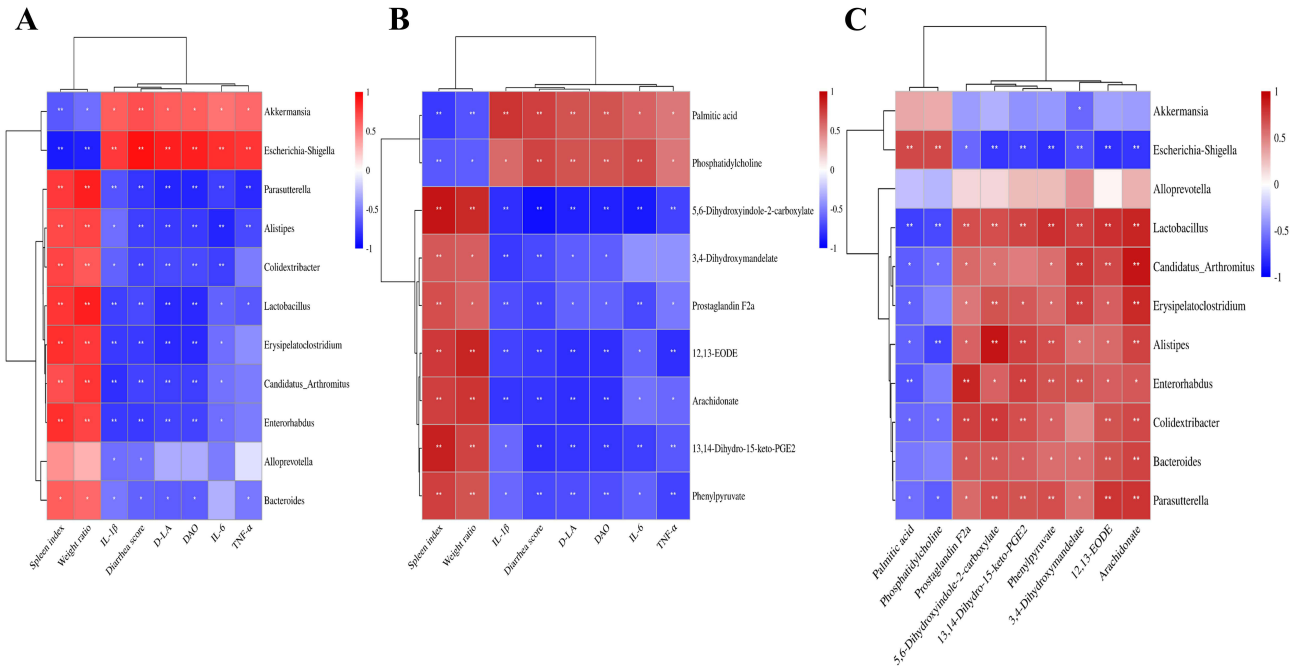

Figure 5 Correlation analysis was conducted between the identified pathway related metabolites in feces, phenotype (PT) and gut microbiota data. (**A**) The correlation analysis results between gut microbiota and PT data. (**B**) The correlation analysis results between fecal metabolomics data and PT data. (**C**) The correlation analysis results between fecal metabolomics data and gut microbiota data. The data were expressed in means ± SEM. *$P < 0.05$, **$P < 0.01$.

major components of MagO and CIM-related targets. These 51 genes were further analyzed using the STRING database, and a protein-protein interaction (PPI) network was constructed in Cytoscape to elucidate MagO's therapeutic effects on 5-FU-induced mucositis (Figure 6C and D). Additionally, using the CentiScaPe 2.2 plugin and applying thresholds (Degree > 8.7346939, Closeness > 0.0100395, Betweenness > 54.0000001), 12 core targets were identified.

Subsequently, GO enrichment analysis was performed across Biological Process (BP), Cellular Component (CC), and Molecular Function (MF) categories, resulting in the identification of 10 significantly enriched biological terms. As shown in Figure 6E, the analysis revealed strong associations with biological processes such as the regulation of regulation of epithelial cell apoptotic process, regulation of lipid transport, regulation of inflammatory response and positive regulation of fatty acid metabolic process. Additionally, KEGG enrichment analysis identified the top 15 significantly enriched pathways (Figure 6F), with notable pathways including pathways in cancer, chemical carcinogenesis - receptor activation, lipid and atherosclerosis, and the PI3K/AKT signaling pathway. Recent studies suggested that PI3K/AKT signaling pathway was closely related to CIM, suggesting that MagO might exert its therapeutic effects against 5-FU-induced mucositis through this pathway.[27,28] Therefore, the PI3K/AKT signaling pathway was selected as the focus for further mechanistic validation.

MagO Regulated Key Targets in the PI3K/AKT Signaling Pathway

Among the 12 core targets, those involved in the PI3K-AKT signaling pathway include JAK2, PIK3CA, PRKCA, and RXRA. Therefore, this study utilized molecular docking methods to analyze the interactions between the five core components of MagO (β-eudesmol, α-eudesmol, γ-eudesmol, aristolochene and α-selinene) and these four core targets. Lower binding energy indicated a more stable ligand-receptor binding, as reflected in the docking scores. Previous studies suggested that a binding score below −5.0 kcal/mol indicated good binding activity between the ligand and receptor.[29] Figure 7A presented a heatmap of the docking scores, highlighting strong binding activity and stable complex formation. Figure 7B displayed the docking structures with higher docking scores.

To further verify whether MagO exerted its effects through the regulation of these key targets in the 5-FU-mediated response, RT-qPCR was used to assess the mRNA expressions of these targets. As shown in Figure 7C, compared to the

https://doi.org/10.2147/DDDT.S515605

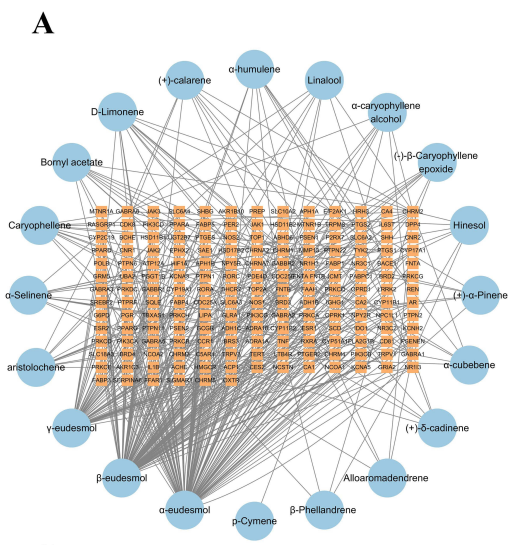

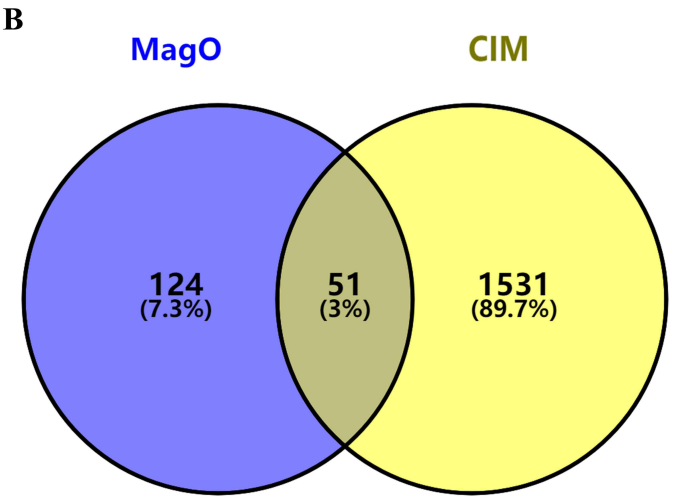

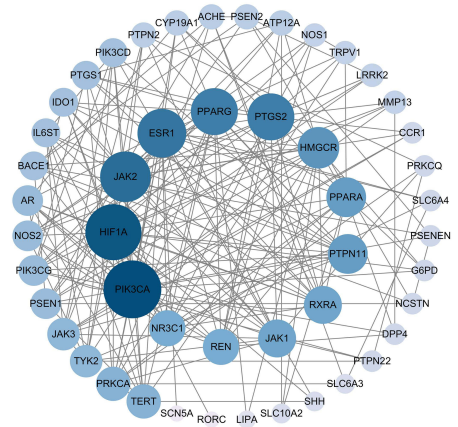

D

Table.1 Analysis of key targets

Target	Degree unDir	Betweenness unDir	Closeness unDir
PIK3CA	24	370.7691328	0.01369863
HIF1A	23	290.4666375	0.013157895
JAK2	20	181.7221931	0.012658228
ESR1	19	196.9441051	0.012345679
PTGS2	18	144.8012177	0.012345679
PPARG	18	126.4180543	0.012195122
HMGCR	15	161.2041894	0.011904762
PPARA	14	100.6450194	0.011627907
PTPN11	14	73.96803988	0.011363636
RXRA	13	72.60798448	0.011627907
TERT	11	72.11901432	0.011627907
PRKCA	11	112.5785922	0.011363636

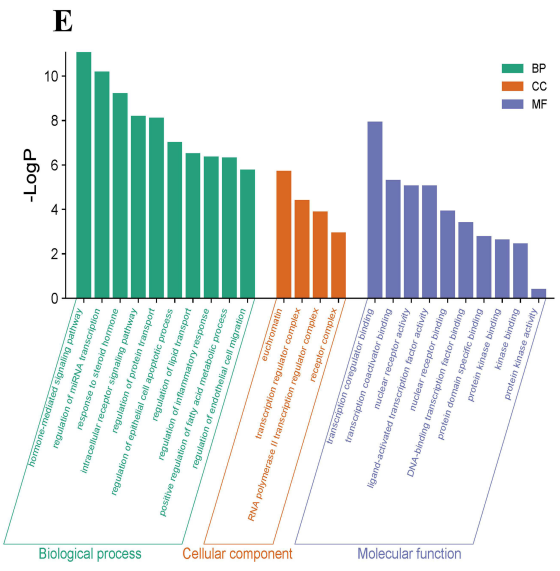

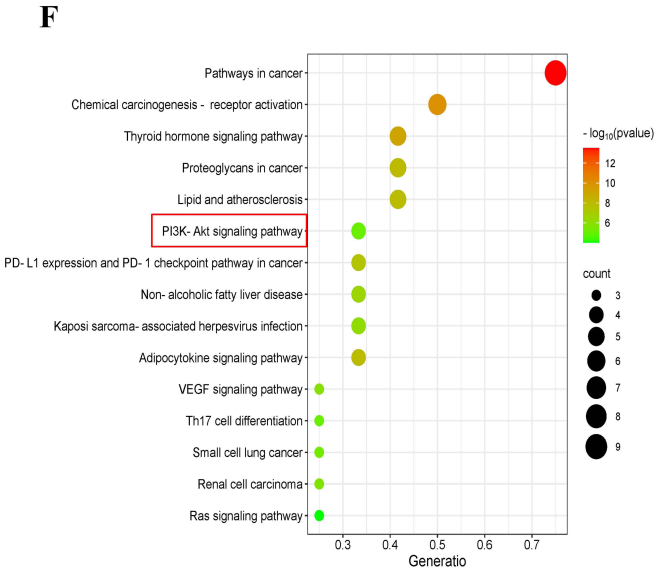

Figure 6 Network Pharmacology analysis. (**A**) The "components–targets" interaction network. (**B**) MagO and CIM intersection target Venn diagram. (**C**) PPI network of potential targets. (**D**) Table.1 Analysis of key targets. (**E**) GO enrichment analysis of potential targets. (**F**) KEGG pathway enrichment analysis.
Abbreviations: BP, biological process; CC, cellular component; MF, molecular function.

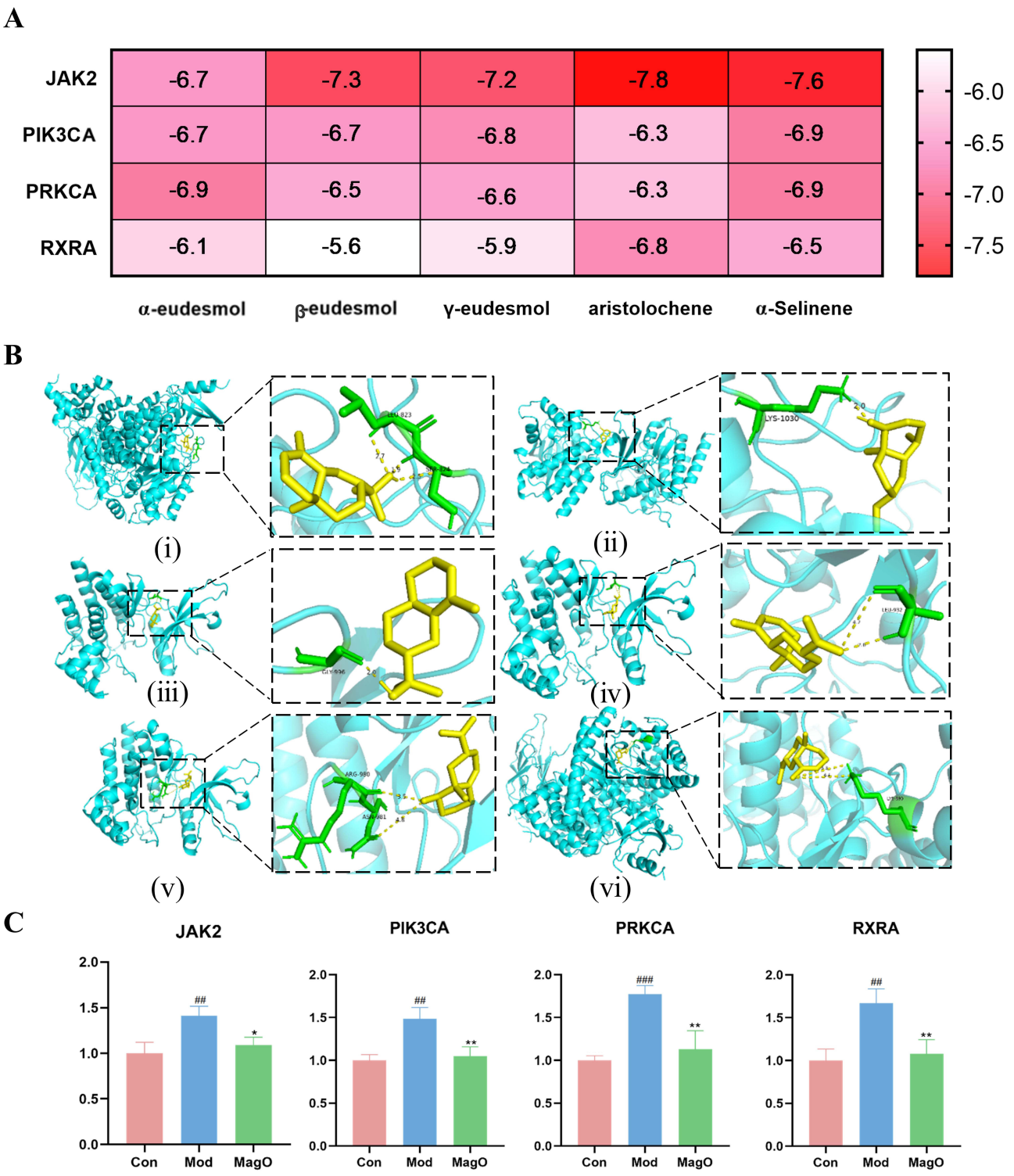

Figure 7 The docking results and validation results of key targets in the docking model. (**A**)The molecular docking score heat map of key targets. (**B**) Molecular docking diagram of key targets binding energy. (i) PIK3CA and α-edudesmol. (ii) JAK2 and β-eudesmol. (iii) JAK2 and γ-eudesmol. (iv) JAK2 and α-Selinene. (v) JAK2 and aristolochene. (vi) PIK3CA and a-Selinene. (**C**)The mRNA expressions of JAK2, PIK3CA, PRKCA and RXRA. The data were expressed in means ± SEM. $^{*}P < 0.05$, $^{**}P < 0.01$vs. Mod group; $^{\#\#}P < 0.01$, $^{\#\#\#\#}P < 0.001$ vs Con group.

https://doi.org/10.2147/DDDT.S515605

Con group, the mRNA expressions of JAK2, PIK3CA, PRKCA, and RXRA were significantly downregulated following 5-FU treatment (P <0.01, P <0.01, P <0.001 and P <0.01, respectively), whereas MagO treatment significantly reversed these changes. These results suggested that MagO could exert protective effects in the pathological process induced by 5-FU by modulating expressions of these core genes.

Integrative Analysis of Network Pharmacology and Metabolomics

Through the integration of 68 differential metabolites and 51 shared genes, a total of 189 related pathways were enriched. After screening, the top 25 significantly enriched pathways were retained and visualized in a bar chart (Figure 8). These pathways included the PI3K-AKT signaling pathway, HIF-1 signaling pathway, JAK-STAT signaling pathway, Chemokine signaling pathway, Th17 cell differentiation, and VEGF signaling pathway. Among these, the PI3K-AKT signaling pathway has been shown to play a crucial role not only in maintaining intestinal barrier function but also in the occurrence and regulation of intestinal mucosal inflammation. Therefore, this study, combined with the results of network pharmacology analysis, further confirmed the critical impact of differential metabolites on intestinal inflammation, particularly through the regulation of the PI3K-AKT signaling pathway, contributing to the development and progression of intestinal mucosal inflammation.

MagO Inhibited the PI3K/AKT Pathway, Reduced Expressions of Tight Junctional Proteins and Apoptosis-Related Proteins

The above results suggested that 5-FU might influence mucosal repair and the regulation of apoptosis by inhibiting the PI3K/AKT signaling pathway. Western blot and immunohistochemistry analysis indicated that in the ileum tissues of 5-FU-induced mice, MagO significantly reversed expressions of ZO-1 and Occludin, showing a statistically significant difference compared to the Mod group (P < 0.001, P < 0.001; P <0.01, P <0.05) (as shown in Figure 9A and B). As depicted in Figure 9C, the MagO treatment group significantly reduced expression of Bax (P < 0.05) while significantly increasing expression of the Bcl-2 (P < 0.01). Additionally, Figure 9D showed that, compared to the Mod group, MagO significantly inhibited expressions of P-PI3K/PI3K and P-AKT/AKT (P < 0.05, P < 0.05). These findings indicated that MagO could reduce apoptosis and protect the intestinal mucosa from damage by inhibiting the PI3K/AKT signaling pathway.

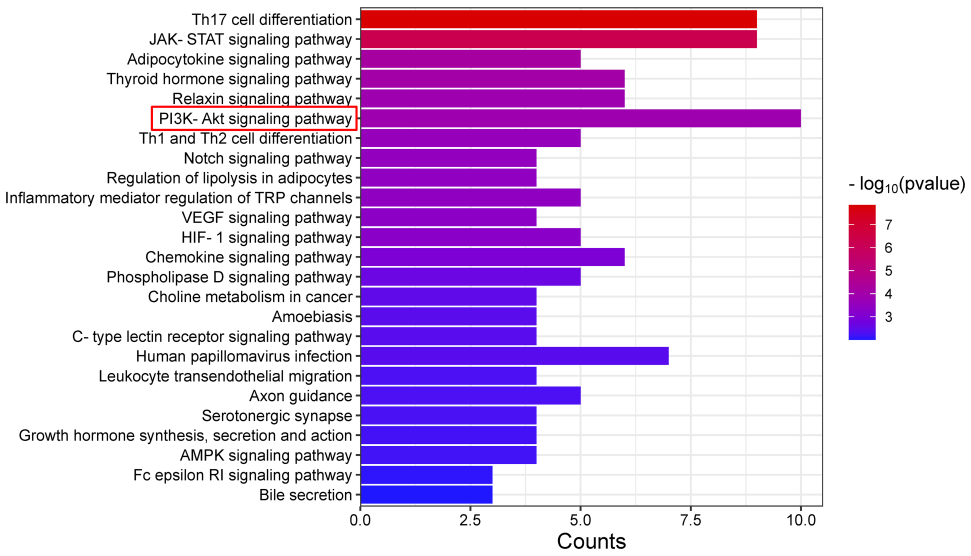

Figure 8 Integrative Analysis of Network Pharmacology and Metabolomics. The bar Chart Showing the Top 25 Enriched KEGG Pathways (Ranked by -log10(p value)).

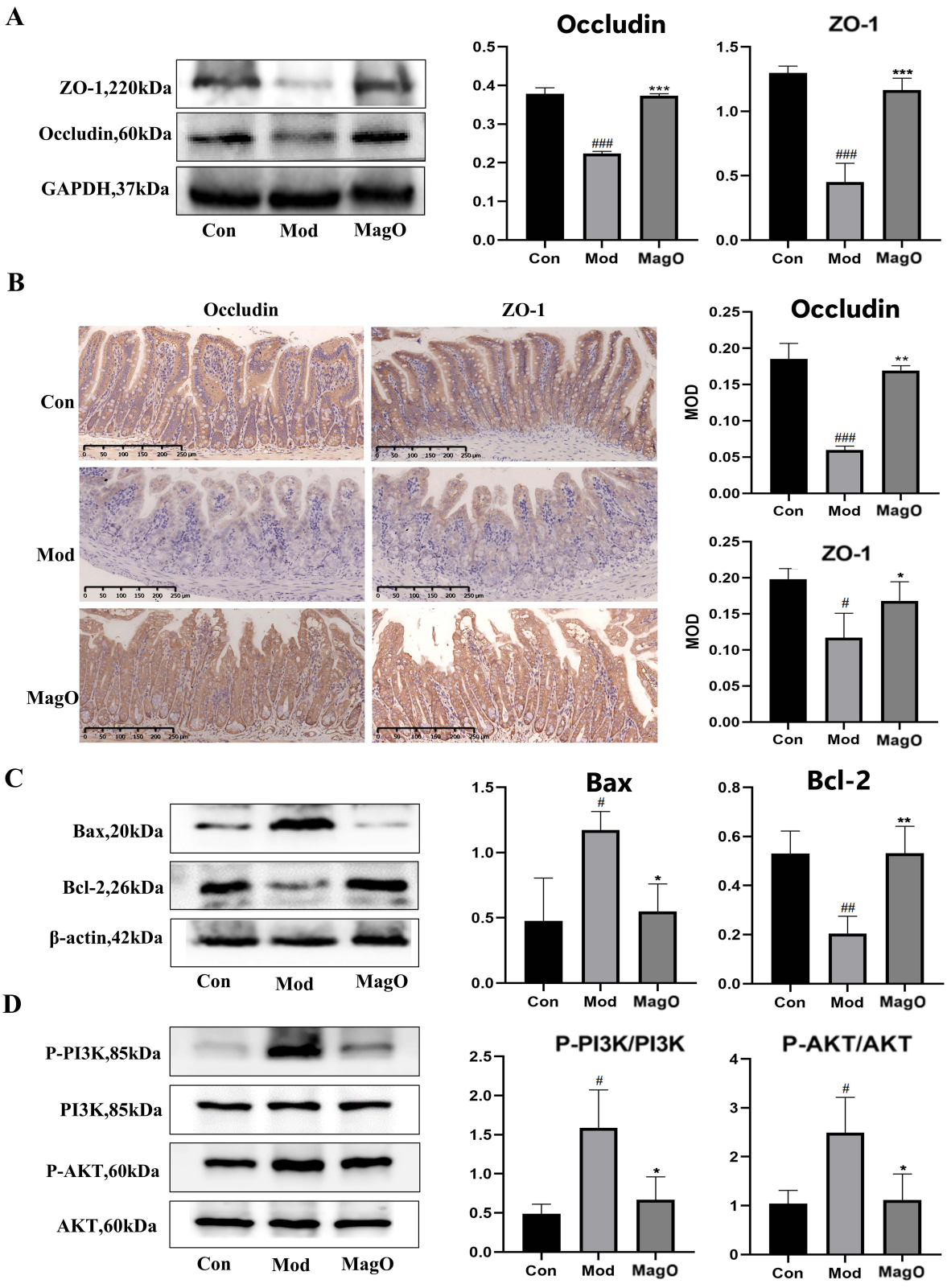

Figure 9 MagO induced the inhibition of the PI3K/AKT pathway and reduced the expression of tight junctional proteins and apoptosis. (**A**) MagO regulated expressions of ZO-1 and Occludin in ileum tissue (WB). (**B**) MagO regulated expressions of Occludin and ZO-1 (IHC, n = 3 per group); scale bar, 250μm. (**C**)MagO regulated expressions of Bax and Bcl-2 in ileum tissue. (**D**) MagO regulated expressions of P-PI3K/PI3K and P-AKT and AKT in ileum tissue. The data were expressed in means ± SEM. $^{*}P < 0.05$, $^{**}P < 0.01$, $^{***}P < 0.001$ vs the Mod group; $^{\#}P < 0.05$, $^{\#\#}P < 0.01$, $^{\#\#\#}P < 0.001$ vs the Con group.

https://doi.org/10.2147/DDDT.S515605

Discussion

This study successfully established a 5-FU-induced mucositis mouse model. Given that weight loss, spleen weight reduction, and diarrhea are common side effects of 5-FU chemotherapy, these parameters were used to assess the severity of mucositis.[30,31] The results demonstrated that MagO (100 μL·kg^{-1}) significantly increased body weight and spleen index in mucositis mice, reduced diarrhea scores, and alleviated 5-FU-induced ileum morphological damage, such as villus atrophy, crypt destruction, and inflammatory infiltration. However, the medium dose (50 μL·kg^{-1}) and low dose (25 μL·kg^{-1}) did not significantly improve intestinal mucositis. Although a dose-dependent trend was observed, the differences were not statistically significant compared to the Mod group. Damage to the intestinal epithelial barrier is a critical pathogenic factor in 5-FU-induced mucositis. The study found that MagO-H significantly reduced levels of inflammatory cytokines TNF-α, IL-6, and IL-1β in the serum of 5-FU-induced mice, as well as levels of intestinal permeability markers DAO and D-LA. This indicated that MagO-H effectively alleviated the intestinal permeability and inflammatory responses associated with impaired epithelial barrier function. Given that only MagO-H exhibited significant protective effects against 5-FU-induced mucositis among the three doses tested, it was selected for further mechanistic studies.

Gut microbiota plays a critical role in the pathogenesis of intestinal mucositis.[32] Studies have shown that 5-FU influences the development of mucositis by altering the gut microbiome.[33,34] To investigate whether the gut microbiota is involved in the therapeutic effects of MagO on 5-FU-induced CIM, we analyzed the gut microbiota composition following 5-FU and MagO treatment. The results indicated that MagO reversed the 5-FU-induced reduction in gut microbiota abundance and diversity, significantly enriching the relative abundance of beneficial bacteria such as *Lactobacillus, Bacteroides, Alistipes, Alloprevotella* and *Parasuttella*. The enrichment of these bacteria contributes to the restoration of intestinal barrier function and the alleviation of inflammation.[19,35–38] Conversely, pathogenic bacteria promote the progression of intestinal mucositis. *Shigella*, for example, is associated with well-defined diseases and triggers infectious colitis.[39] In our study, MagO significantly reversed the 5-FU-induced increase in the relative abundance of *Escherichia-Shigella*, suggesting that the alleviation of CIM by MagO could be mediated through the inhibition of pathogenic bacteria. Previous studies have demonstrated that metabolites play a crucial role in the development of intestinal mucositis.[40]

Through non-targeted metabolomic analysis of mouse feces, we found that MagO significantly influenced the metabolites in the feces of 5-FU-treated mice, particularly those related to fatty acids and amino acids. These changes affected several metabolic pathways, including arachidonic acid metabolism, linoleic acid metabolism, and the biosynthesis of phenylalanine, tyrosine, and tryptophan. Among these altered pathways, arachidonic acid metabolism was the most prominent and is closely associated with intestinal barrier function and homeostasis.[41–43] Our findings indicated that MagO modulated regulation within the arachidonic acid metabolic pathway, including the upregulation of arachidonic acid, prostaglandinF2α, prostaglandinA2, and 13,14-Dihydro-keto-prostaglandinE2 levels, along with the downregulation of phosphatidylcholine levle. PGE2 is a key lipid signaling molecule widely involved in tissue regeneration and repair, particularly in the intestine, where it plays a regulatory role in intestinal perfusion by modulating blood flow and promoting homeostasis, especially through its receptor-mediated actions.[44,45] Additionally, PGE2 accelerates the repair of 5-FU-induced intestinal damage by upregulating FOXM1 expression and the expression of cyclins D1 and D2.[46] Studies have shown that PGE2 exerts protective effects on the gastrointestinal mucosa through its EP receptors.[47] Specifically, activation of the EP4 receptor in intestinal epithelial cells contributes to maintaining intestinal homeostasis. In a DSS-induced colitis mouse model, PGE2 alleviates intestinal inflammation and promotes the regeneration of the intestinal epithelial barrier via modulation of the EP4 receptor.[48] Additionally, PGE2 enhances the healing of small intestinal lesions by upregulating vascular endothelial growth factor (VEGF) expression and stimulating angiogenesis through EP4 receptor activation.[49] The EP2 receptor is also considered a potential therapeutic target for intestinal inflammation.[50–52] Research indicates that PGE2, by binding to the EP2 receptor, reduces radiation-induced apoptosis of small intestinal epithelial cells and increases crypt survival, a process involving the PI3K/AKT signaling pathway.[53] Our study demonstrated that MagO administration significantly reversed 5-FU-induced downregulation of PGE2 level, EP2 and EP4 protein expressions, indicating its intestinal epithelial barrier protection through modulation of the PGE2/EP2/EP4 signaling axis. We also conducted correlation analyses of phenotypic, gut microbiota, and metabolomic data to identify significant associations between key bacterial genera and metabolic pathways. Results showed that relative abundances of *Lactobacillus, Alistipes, Parasuttella and Escherichia-Shigella* were significantly correlated with levels of arachidonic acid metabolites and phenotypic indicators. The findings indicated that MagO alleviated 5-FU-induced

intestinal mucositis by restoring gut microbiota-metabolite homeostasis, enabling key microbiota to ameliorate mucosal damage through regulation of the arachidonic acid metabolic network.

To further investigate the mechanism underlying MagO's therapeutic effects on CIM, this study also employed network pharmacology approaches. GC-MS analysis revealed 20 chemical components of MagO were identified, corresponding to CIM targets, resulting in the identification of 51 overlapping targets. A "compound-target" network was subsequently constructed. The results indicated that β-eudesmol, α-eudesmol, γ-eudesmol, aristolochene, and α-selinene were the key components of MagO responsible for amelioration of 5-FU-induced CIM. KEGG pathway analysis suggested that MagO exerted its effects by modulating the PI3K/AKT signaling pathway. To validate the impact of MagO on the PI3K/AKT pathway, molecular docking was conducted to analyze the interactions between the five core components and key targets involved in the PI3K/AKT pathway (JAK2, PIK3CA, PRKCA, and RXRA). Furthermore, RT-qPCR was used to verify the expressions of these targets. The results demonstrated that MagO modulated the expression of these core genes. The PI3K/AKT signaling pathway is closely associated with the development of intestinal mucositis. Studies have shown that activation of this pathway can induce pro-inflammatory and pro-apoptotic signals, while downregulating the expression of tight junction proteins, thereby contributing to mucosal damage.[54–56] Western blot and immunohistochemistry analysis revealed that MagO inhibited the PI3K/AKT pathway, downregulated Bax expression, upregulated Bcl-2 expression, and increased ZO-1 and Occludin expressions.

Notably, MagO-M showed efficacy in the intestinal permeability indexes but failed to improve other pharmacological indexes. This may be because its lipophilic components accumulate preferentially in the intestine after oral administration, failing to reach the threshold to inhibit spleen-related action or regulate systemic inflammatory factors.[57,58] Thus, increasing the drug concentration is essential for both local and systemic therapeutic effects. Moreover, MagO, a multi-component mixture containing terpenoids like β-eudesmol, α-pinene, and β-caryophyllene, is rapidly absorbed and distributed after oral administration, with the highest gastrointestinal exposure.[57–60] Hepatic metabolism converts its components into more polar metabolites, and excretion mainly occurs via urine and feces.[57–60] Due to its complexity, volatility, and lipophilicity, MagO's average bioavailability is 1.54% ~55%.[59,61–64] MagO is safe and low-toxic within a certain dose range, but certain components at high doses such as α-pinene, D-Limonene and Linalool may cause hepatotoxicity, and long-term use might result in gastrointestinal discomfort.[20,65–67] Caution is needed in determining dosage and treatment duration to ensure clinical safety. Additionally, male mice were chosen to avoid estrogen interference in intestinal mucositis development, ensuring experimental reliability.[68]

In summary, MagO, as the core active component of the traditional Chinese herb Magnoliae Officinalis Cortex, had been demonstrated for the first time to exert mucosal protective effects through a multidimensional "microbiota-metabolism-signaling pathway" synergistic network. Specifically, MagO not only selectively enriched beneficial bacteria associated with intestinal mucositis, while suppressing pathogenic bacteria, but also remodeled the arachidonic acid metabolic network and concurrently inhibited the PI3K/AKT signaling pathway. This established a triple protective network involving microbial remodeling, metabolic regulation, and cellular signaling intervention. Methodologically, our integrated multi-omics analysis combined with GC-MS profiling had revealed, for the first time, that MagO's core components directly targeted host cell pathways while indirectly promoting mucosal repair through microbiota-derived metabolites. These findings provided scientific evidence for the clinical application of Magnoliae Officinalis Cortex components in modern medicine and pave a novel pathway for developing long-acting and safe therapeutic strategies against CIM.

Conclusion

In summary, we elucidated the pharmacological effects and molecular mechanisms by which MagO ameliorated 5-FU-induced intestinal mucositis through integrated gut microbiota analysis, metabolomics, and network pharmacology. Mechanistically, MagO restored the balance of gut microbiota and metabolites. Additionally, MagO enhanced the expression of tight junction proteins, mitigated damage to the intestinal epithelial barrier, reduced intestinal permeability, and suppressed apoptosis. It was noteworthy that the effects of MagO might mediated by inhibition of the PI3K/AKT pathway and activation of the PGE2/EP2/EP4 pathway (Figure 10). These integrated approaches provide robust evidence

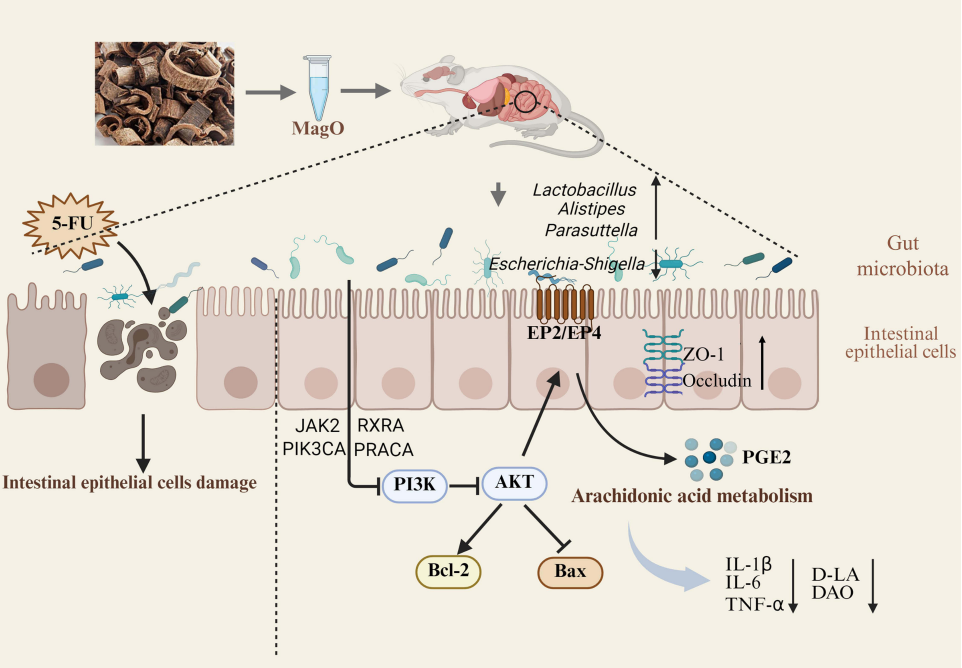

Figure 10 MagO exerted its inhibitory effects against the epithelial barrier damage caused by 5-FU. Firstly, Mag restored the 5-FU-induced alterations in gut microbiota by upregulating relative abundances of beneficial bacteria such as *Lactobacillus, Alistipes and Parasuttella*, while downregulating that of pathogenic *Escherichia-Shigella*. Secondly, MagO influenced various metabolic pathways, particularly arachidonic acid metabolism, and was found to upregulate PGE2 level andexpressions of EP2 and EP4. Additionally, MagO targeted JAK2, PIK3CA, PRKCA, and RXRA to inhibit the PI3K/AKT pathway, thereby upregulating Bcl-2 expression and downregulating Bax expression. These actions ultimately enhanced expressions of tight junction proteins ZO-1 and Occludin.

for MagO's protective role against CIM by modulating key biological pathways and gut microbiota, establishing a framework for clinical translation and mechanistic exploration.

Abbreviations

CIM, Chemotherapy-induced mucositis; MagO, Magnoliae Officinalis Cortex volatile oil; 5-FU, 5-fluorouracil; DAO, diamine oxidase; D-LA, D-lactic acid; OUT, operational taxonomic units; PCA, Principal component analysis; PLS-DA, partial least squares discriminant analysis; VIP, Variable Importance in the Projection; FC, Fold Change; PPI, protein-protein interaction; ZO-1, zonula occludens 1; PGE2, prostaglandin E2; EP, prostaglandin receptor.

Data Sharing Statement

The datasets PRJNA1198729 for this study can be found in the National Center for Biotechnology Information (NCBI). SRA records will be accessible with the following link: https://www.ncbi.nlm.nih.gov/sra/PRJNA1198729.

Ethics Statement

The Animal Research Ethics Committee of the Laboratory Animals Center of Chengdu University of Traditional Chinese Medicine approved all procedures following the 391 recommendations presented in the Guide for the Care and Use of Laboratory Animals (2022007021).

Acknowledgments

This work was supported by Program of National Natural Science Foundation of China (81503272, 81630101, 81891012), Application Foundation Research Project of Sichuan Provincial Department of Science and Technology (2017JY0187), Xinglin Scholar Research Premotion Project of Chengdu University of TCM (2018016), the Regional Joint Fund of the National Natural Science Foundation of China: Study on the Geoherbalism of Medicinal Materials from Sichuan Tract (U19A2010), National Interdisciplinary Innovation Team of Traditional Chinese Medicine: Multi-

dimensional evaluation and multi-disciplinary cross-innovation team of traditional Chinese medicine resources with Southwest characteristics (ZYYCXTD-D-202209), Sichuan Traditional Chinese Medicine Technology Industry Innovation Team: Multidimensional Evaluation of Characteristic Traditional Chinese Medicine Resources and Product Development Innovation Team (2022C001), Sichuan Provincial Administration of Traditional Chinese Medicine Project (2020JC0031, 2024ZD02, 2024MS562).

Author Contributions

All authors made a significant contribution to the work reported, whether that is in the conception, study design, execution, acquisition of data, analysis and interpretation, or in all these areas; took part in drafting, revising or critically reviewing the article; gave final approval of the version to be published; have agreed on the journal to which the article has been submitted; and agree to be accountable for all aspects of the work.

Disclosure

The authors declare that they have no competing interests.

References

1. Mohammed AI, Celentano A, Paolini R, et al. Characterization of a novel dual murine model of chemotherapy-induced oral and intestinal mucositis. *Sci Rep*. 2023;13(1). doi:10.1038/s41598-023-28486-3
2. Van Sebille YZA, Stansborough R, Wardill HR, Bateman E, Gibson RJ, Keefe DM. Management of mucositis during chemotherapy: from pathophysiology to pragmatic therapeutics. *Curr Oncol Rep*. 2015;17(11):50. doi:10.1007/s11912-015-0474-9
3. Stringer AM, Gibson RJ, Bowen JM, Logan RM, Yeoh ASJ, Keefe DMK. Chemotherapy-induced mucositis: the role of gastrointestinal microflora and mucins in the luminal environment. *J Support Oncol*. 2007;5(6):259–267.
4. Wisinski K, Benson A. Chemotherapy-induced mucositis: focusing on diarrhea. *J Support Oncol*. 2007;5(6):270–271.
5. Mindt S, Aida S, Merx K, et al. Therapeutic drug monitoring (TDM) of 5-fluorouracil (5-FU): new preanalytic aspects. *Clin Chem Lab Med*. 2019;57(7):1012–1016. doi:10.1515/cclm-2018-1177
6. Vodenkova S, Buchler T, Cervena K, Veskrnova V, Vodicka P, Vymetalkova V. 5-fluorouracil and other fluoropyrimidines in colorectal cancer: past, present and future. *Pharmacol Ther*. 2020;206:107447. doi:10.1016/j.pharmthera.2019.107447
7. Yuan J, Khan SU, Yan J, Lu J, Yang C, Tong Q. Baicalin enhances the efficacy of 5-Fluorouracil in gastric cancer by promoting ROS-mediated ferroptosis. *Biomed Pharmacother Biomedecine Pharmacother*. 2023;164:114986. doi:10.1016/j.biopha.2023.114986
8. Wigmore PM, Mustafa S, El-Beltagy M, Lyons L, Umka J, Bennett G. Effects of 5-FU. *Adv Exp Med Biol*. 2010;678:157–164. doi:10.1007/978-1-4419-6306-2_20
9. Hamouda N, Sano T, Oikawa Y, et al. Apoptosis, dysbiosis and expression of inflammatory cytokines are sequential events in the development of 5-fluorouracil-induced intestinal mucositis in mice. *Basic Clin Pharmacol Toxicol*. 2017;121(3):159–168. doi:10.1111/bcpt.12793
10. Duncan M, Grant G. Oral and intestinal mucositis - causes and possible treatments. *Aliment Pharmacol Ther*. 2003;18(9):853–874. doi:10.1046/j.1365-2036.2003.01784.x
11. Longley DB, Harkin DP, Johnston PG. 5-fluorouracil: mechanisms of action and clinical strategies. *Nat Rev Cancer*. 2003;3(5):330–338. doi:10.1038/nrc1074
12. Ribeiro RA, Wanderley CWS, Wong DVT, et al. Irinotecan- and 5-fluorouracil-induced intestinal mucositis: insights into pathogenesis and therapeutic perspectives. *Cancer Chemother Pharmacol*. 2016;78(5):881–893. doi:10.1007/s00280-016-3139-y
13. Logan RM, Stringer AM, Bowen JM, Gibson RJ, Sonis ST, Keefe DMK. Is the pathobiology of chemotherapy-induced alimentary tract mucositis influenced by the type of mucotoxic drug administered? *Cancer Chemother Pharmacol*. 2009;63(2):239–251. doi:10.1007/s00280-008-0732-8
14. Gan Y, Ai G, Wu J, et al. Patchouli oil ameliorates 5-fluorouracil-induced intestinal mucositis in rats via protecting intestinal barrier and regulating water transport. *J Ethnopharmacol*. 2020;250:112519. doi:10.1016/j.jep.2019.112519
15. Wang J, Feng W, Zhang S, et al. Ameliorative effect of Atractylodes macrocephala essential oil combined with Panax ginseng total saponins on 5-fluorouracil induced diarrhea is associated with gut microbial modulation. *J Ethnopharmacol*. 2019;238:111887. doi:10.1016/j.jep.2019.111887
16. Liu D, Tang F, Zhang L, et al. Alpinia katsumadai hayata volatile oil is effective in treating 5-fluorouracil-induced mucositis by regulating gut microbiota and modulating the GC/GR pathway and the mPGES-1/PGE2/EP4 pathways. *J Agric Food Chem*. 2023;71(41):15156–15169. doi:10.1021/acs.jafc.3c05051
17. Zhang T, Lu SH, Bi Q, et al. Volatile oil from amomi fructus attenuates 5-fluorouracil-induced intestinal mucositis. *Front Pharmacol*. 2017;8:786. doi:10.3389/fphar.2017.00786
18. Wu Q, Wei D, Dong L, et al. Variation in the microbial community contributes to the improvement of the main active compounds of Magnolia officinalis Rehd. et Wils in the process of sweating. *Chin Med*. 2019;14:45. doi:10.1186/s13020-019-0267-4
19. Xie Q, Li H, Ma R, et al. Effect of Coptis chinensis franch and Magnolia officinalis on intestinal flora and intestinal barrier in a TNBS-induced ulcerative colitis rats model. *Phytomedicine Int J Phytother Phytopharm*. 2022;97:153927. doi:10.1016/j.phymed.2022.153927
20. Poivre M, Duez P. Biological activity and toxicity of the Chinese herb *Magnolia officinalis* Rehder & E. Wilson (Houpo) and its constituents. *J ZHEJIANG Univ-Sci B*. 2017;18(3):194–214. doi:10.1631/jzus.B1600299
21. Zhao L, Xiao HT, Mu HX, et al. Magnolol, a natural polyphenol, attenuates dextran sulfate sodium-induced colitis in mice. *Mol*. 2017;22(7):1218. doi:10.3390/molecules22071218
22. Pang YL, Han XF, Bamikole MA, et al. Anti-diarrhea and anti-oxidant properties of Magnolol. *Trop J Pharm Res*. 2013;12(1):85–91. doi:10.4314/tjpr.v12i1.14

23. Chan SSK, Zhao M, Lao L, Fong HH, Che CT. Magnolol and honokiol account for the anti-spasmodic effect of Magnolia officinalis in isolated Guinea pig ileum. *Planta Med*. 2008;74(4):381–384. doi:10.1055/s-2008-1034320
24. Li S, Huang Y, Liu L, Zhang F, Ao H, Luo Y. Mechanism of Magnolia volatile oil in the treatment of acute pancreatitis based on GC-MS, network pharmacology, and molecular docking. *Evid-Based Compl Altern Med ECAM*. 2023;2023:3503888. doi:10.1155/2023/3503888
25. Zhang Q, Zhang R, Deng H, et al. Antioxidant activity of volatile oil contained in Chinese medicine Houpao before and after processing and sweating and its efficacy in the treatment of ulcerative colitis in Chinese medicine. *Chin Arch Trad Chin Med*. 2024;42(8):180–185, 291–294. doi:10.13193/j.issn.1673-7717.2024.08.036
26. Kurita A, Kado S, Kaneda N, Onoue M, Hashimoto S, Yokokura T. Modified irinotecan hydrochloride (CPT-11) administration schedule improves induction of delayed-onset diarrhea in rats. *Cancer Chemother Pharmacol*. 2000;46(3):211–220. doi:10.1007/s002800000151
27. Bai X, Deng J, Duan Z, et al. Ginsenoside Rh4 alleviates gastrointestinal mucositis and enhances chemotherapy efficacy through modulating gut microbiota. *Phytomedicine Int J Phytother Phytopharm*. 2024;128. doi:10.1016/j.phymed.2024.155577
28. Huang N, Wei Y, Wang M, et al. Dachaihu decoction alleviates septic intestinal epithelial barrier disruption via PI3K/AKT pathway based on transcriptomics and network pharmacology. *J Ethnopharmacol*. 2025;337(Pt 3). doi:10.1016/j.jep.2024.118937
29. Zhu W, Li Y, Zhao J, Wang Y, Li Y, Wang Y. The mechanism of triptolide in the treatment of connective tissue disease-related interstitial lung disease based on network pharmacology and molecular docking. *Ann Med*. 2022;54(1):541–552. doi:10.1080/07853890.2022.2034931
30. Du K, Wang L, Wang Z, et al. Angelica Sinensis polysaccharide antagonizes 5-Fluorouracil-induced spleen injury and dysfunction by suppressing oxidative stress and apoptosis. *Biomed Pharmacother Biomedecine Pharmacother*. 2023;162:114602. doi:10.1016/j.biopha.2023.114602
31. Alvarez P, Antonio Marchal J, Boulaiz H, et al. 5-Fluorouracil derivatives: a patent review. *EXPERT Opin Ther Pat*. 2012;22(2):107–123. doi:10.1517/13543776.2012.661413
32. Qiu P, Ishimoto T, Fu L, Zhang J, Zhang Z, Liu Y. The gut microbiota in inflammatory bowel disease. *Front Cell Infect Microbiol*. 2022;12:733992. doi:10.3389/fcimb.2022.733992
33. Li HL, Lu L, Wang XS, et al. Alteration of gut microbiota and inflammatory cytokine/chemokine profiles in 5-fluorouracil induced intestinal mucositis. *Front Cell Infect Microbiol*. 2017;7:455. doi:10.3389/fcimb.2017.00455
34. Alexander JL, Wilson ID, Teare J, Marchesi JR, Nicholson JK, Kinross JM. Gut microbiota modulation of chemotherapy efficacy and toxicity. *Nat Rev Gastroenterol Hepatol*. 2017;14(6):356–365. doi:10.1038/nrgastro.2017.20
35. Kang L, Pang J, Zhang X, et al. L-arabinose attenuates LPS-induced intestinal inflammation and injury through reduced M1 macrophage polarization. *J Nutr*. 2023;153(11):3327–3340. doi:10.1016/j.tjnut.2023.09.012
36. Roy S, Dhaneshwar S. Role of prebiotics, probiotics, and synbiotics in management of inflammatory bowel disease: current perspectives. *WORLD J Gastroenterol*. 2023;29(14):2078–2100. doi:10.3748/wjg.v29.i14.2078
37. Wang C, Zhao J, Zhang H, Lee YK, Zhai Q, Chen W. Roles of intestinal bacteroides in human health and diseases. *Crit Rev Food Sci Nutr*. 2021;61(21):3518–3536. doi:10.1080/10408398.2020.1802695
38. Brown EM, Ke X, Hitchcock D, et al. Bacteroides-derived sphingolipids are critical for maintaining intestinal homeostasis and symbiosis. *Cell Host Microbe*. 2019;25(5):668–680.e7. doi:10.1016/j.chom.2019.04.002
39. Dekker JP, Frank KM. Salmonella, Shigella, and yersinia. *Clin Lab Med*. 2015;35(2):225–246. doi:10.1016/j.cll.2015.02.002
40. Fu Y, Lyu J, Wang S. The role of intestinal microbes on intestinal barrier function and host immunity from a metabolite perspective. *Front Immunol*. 2023;14:1277102. doi:10.3389/fimmu.2023.1277102
41. Zhu J, Liu W, Bian Z, et al. Lactobacillus plantarum zhang-LL inhibits colitis-related tumorigenesis by regulating arachidonic acid metabolism and CD22-mediated B-cell receptor regulation. *Nutrients*. 2023;15(21):4512. doi:10.3390/nu15214512
42. Wang Q, Lin Y, Sheng X, et al. Arachidonic acid promotes intestinal regeneration by activating WNT signaling. *Stem Cell Rep*. 2020;15(2):374–388. doi:10.1016/j.stemcr.2020.06.009
43. Xu C, Gu L, Hu L, et al. FADS1-arachidonic acid axis enhances arachidonic acid metabolism by altering intestinal microecology in colorectal cancer. *Nat Commun*. 2023;14(1):2042. doi:10.1038/s41467-023-37590-x
44. Montrose DC, Nakanishi M, Murphy RC, et al. The role of PGE2 in intestinal inflammation and tumorigenesis. *Prostaglandins Other Lipid Mediat*. 2015;116-117:26–36. doi:10.1016/j.prostaglandins.2014.10.002
45. Cheng H, Huang H, Guo Z, Chang Y, Li Z. Role of prostaglandin E2 in tissue repair and regeneration. *Theranostics*. 2021;11(18):8836–8854. doi:10.7150/thno.63396
46. Yue M, Shao L, Cheng J, et al. Prostaglandin E2 accelerated recovery of chemotherapy-induced intestinal damage by increasing expression of cyclin D. *Exp Cell Res*. 2020;388(2):111819. doi:10.1016/j.yexcr.2020.111819
47. Takeuchi K. Prostaglandin EP receptors and their roles in mucosal protection and ulcer healing in the gastrointestinal tract. *Adv Clin Chem*. 2010;51. doi:10.1016/s0065-2423(10)51005-9
48. Na YR, Jung D, Stakenborg M, et al. Prostaglandin E2 receptor PTGER4-expressing macrophages promote intestinal epithelial barrier regeneration upon inflammation. *Gut*. 2021;70(12):2249–2260. doi:10.1136/gutjnl-2020-322146
49. Takeuchi K, Amagase K. Roles of cyclooxygenase, prostaglandin E2 and EP receptors in mucosal protection and ulcer healing in the gastrointestinal tract. *Curr Pharm Des*. 2018;24(18):2002–2011. doi:10.2174/1381612824666180629111227
50. Wu F, Wen Z, Zhi Z, et al. MPGES-1 derived PGE2 inhibits cell migration by regulating ARP2/3 in the pathogenesis of Hirschsprung disease. *J Pediatr Surg*. 2019;54(10):2032–2037. doi:10.1016/j.jpedsurg.2019.01.001
51. Golden J, Illingworth L, Kavarian P, et al. EP2 receptor blockade attenuates COX-2 upregulation during intestinal inflammation. *Shock Augusta Ga*. 2020;54(3):394–401. doi:10.1097/SHK.0000000000001444
52. Yu H, Zhang S, Li R, et al. Berberine alleviates inflammation and suppresses PLA2-COX-2-PGE2-EP2 pathway through targeting gut microbiota in DSS-induced ulcerative colitis. *Biochem Biophys Res Commun*. 2024;695:149411. doi:10.1016/j.bbrc.2023.149411
53. Stenson WF. Prostaglandins and epithelial response to injury. *Curr Opin Gastroenterol*. 2007;23(2):107–110. doi:10.1097/MOG.0b013e3280143cb6
54. Zou P, Yang F, Ding Y, et al. Lipopolysaccharide downregulates the expression of ZO-1 protein through the Akt pathway. *BMC Infect Dis*. 2022;22(1):774. doi:10.1186/s12879-022-07752-1
55. Zhang X, Zhang F, Li Y, et al. Blockade of PI3K/AKT signaling pathway by Astragaloside IV attenuates ulcerative colitis via improving the intestinal epithelial barrier. *J Transl Med*. 2024;22(1):406. doi:10.1186/s12967-024-05168-w

56. Liu C, Zeng Y, Wen Y, Huang X, Liu Y. Natural products modulate cell apoptosis: a promising way for the treatment of ulcerative colitis. *Front Pharmacol*. 2022;13:806148. doi:10.3389/fphar.2022.806148
57. Hakim Yahaya AA, Nuzul Hakimi Wan Salleh WM, Ghani NA, Khamis S, Rezali NS, Aizat Juhari MA. Chemical composition and bioactivities of Magnolia candollii H.Keng essential oil. *Z Naturforschung C J Biosci*. 2022;77(11–12):519–523. doi:10.1515/znc-2022-0100
58. Niu L, Hou Y, Jiang M, Bai G. The rich pharmacological activities of *Magnolia officinalis* and secondary effects based on significant intestinal contributions. *J Ethnopharmacol*. 2021;281:114524. doi:10.1016/j.jep.2021.114524
59. Hou MZ, Chen LL, Chang C, Zan JF, Du SM. Pharmacokinetic and tissue distribution study of eight volatile constituents in rats orally administrated with the essential oil of Artemisiae argyi Folium by GC–MS/MS. *J Chromatogr B*. 2021;1181:122904. doi:10.1016/j.jchromb.2021.122904
60. Zhang R, Yan P, Li Y, Xiong L, Gong X, Peng C. A pharmacokinetic study of patchouli alcohol after a single oral administration of patchouli alcohol or patchouli oil in rats. *Eur J Drug Metab Pharmacokinet*. 2016;41(4):441–448. doi:10.1007/s13318-015-0272-7
61. Chaves JS, Leal PC, Pianowisky L, Calixto JB. Pharmacokinetics and tissue distribution of the sesquiterpene α-humulene in mice. *Planta Med*. 2008;74:1678–1683. doi:10.1055/s-0028-1088307
62. Jeong SH, Jang JH, Cho HY, Lee YB. Simultaneous determination of asarinin, β-eudesmol, and wogonin in rats using ultraperformance liquid chromatography–tandem mass spectrometry and its application to pharmacokinetic studies following administration of standards and Gumiganghwal-tang. *Biomed Chromatogr*. 2021;35(4):e5021. doi:10.1002/bmc.5021
63. Jiang L, Zhang C, Li H. Quantification of β-eudesmol in rat plasma using LC–MS/MS and its application to a pharmacokinetic study. *Biomed Chromatogr*. 2017;31(12):e4023. doi:10.1002/bmc.4023
64. Chi MY, Zhou ZY, Yan T, et al. Quantification of six volatile oil constituents of *Oleum Cinnamomi* in rat plasma and multiple tissues using GC-MS and its application to pharmacokinetic and tissue distribution studies. *J Pharm Biomed Anal*. 2023;223:115128. doi:10.1016/j.jpba.2022.115128
65. Api AM, Belsito D, Botelho D, et al. RIFM fragrance ingredient safety assessment, α-pinene, CAS registry number 80-56-8. *Food Chem Toxicol*. 2022;159:112702. doi:10.1016/j.fct.2021.112702
66. Kim YW, Kim MJ, Chung BY, et al. Safety evaluation and risk assessment of d-Limonene. *J Toxicol Environ Health B Crit Rev*. 2013;16(1):17–38. doi:10.1080/10937404.2013.769418
67. Api AM, Belsito D, Bhatia S, et al. RIFM fragrance ingredient safety assessment, Linalool, CAS registry number 78-70-6. *Food Chem Toxicol Int J Publ Br Ind Biol Res Assoc*. 2015;82(Suppl):S29–38. doi:10.1016/j.fct.2015.01.005
68. Li J, Chen Y, Li S, et al. Estrogen receptor β alleviates colitis by inhibiting ferroptosis in intestinal epithelial cells. *J Inflamm Res*. 2024;17:10785–10805. doi:10.2147/JIR.S492290